PERGAMON

Solid-State Electronics 44 (2000) 147–173

SOLID-STATE ELECTRONICS

Semiconductor lasers for planar integrated optoelectronics

Edward H. Sargent*

Department of Electrical and Computer Engineering, University of Toronto, 10 King's College Road, Toronto, Ont., Canada M5S 3G4

Received 19 July 1999; accepted 18 August 1999

Abstract

We review progress in novel semiconductor lasers positioned to enable planar optoelectronic integration and to facilitate the realization of functional photonic devices. Lateral injection of current into the active region of a semiconductor laser has been pursued, mostly empirically, since the early 1970s. In this work, we focus on recent advances in the development of a device model which accounts for the qualitative structural and operational differences between lateral and conventional vertical injection lasers. We review fabrication methods — both established and emerging — suitable for LCI laser realization. Finally, we report the results of recent combined theoretical–experimental explorations of laser performance.

1. Introduction

1.1. A perspective on semiconductor lasers: present status

Discrete semiconductor lasers are in many respects mature. Over US$1.8 billion worth of semiconductor lasers were sold in 1997 [1]. Semiconductor devices have been developed which lase at room-temperature with the application of as little as 100 μA of continuous current [2]. Once a laser is turned on, additional electrons may be converted into photons with more than 90% efficiency [3]. The width of the spectrum of light from the purest of semiconductor lasers is ten orders of magnitude narrower than its centre frequency; its centre frequency may, in turn, be tuned over a spectral bandwidth eight orders of magnitude greater than its spectral linewidth [4]. The fastest semiconductor lasers are modulated efficiently at rates of over 40 GHz [5].

The maturity of this technology is a consequence of a convergence of factors. There has been consistent growth in the demand for semiconductor lasers in long-distance communications, high density data storage, image recording, materials processing, and medicine. Technological advances have been made as a result of progress in the processing of materials into high-performance devices tailored to particular applications. Continued progress in the understanding of the physical operation of semiconductor lasers, obtained through countless iterations of theoretical development, device fabrication, and experimental probing, has led to the conception, design and implementation of improved devices based on informed choices.

Two paths in the development of the semiconductor laser could represent disruptive, discontinuous jumps: *planar integrated optoelectronic circuits* and *novel functional optoelectronic devices*. These have long been contemplated, but a lack of enabling approaches, devices, and technologies has inhibited progress.

* Tel.: +1-416-946-5051; fax: +1-416-971-3020.
E-mail address: ted.sargent@utoronto.ca (E.H. Sargent).

0038-1101/00/$ - see front matter
PII: S0038-1101(99)00221-X

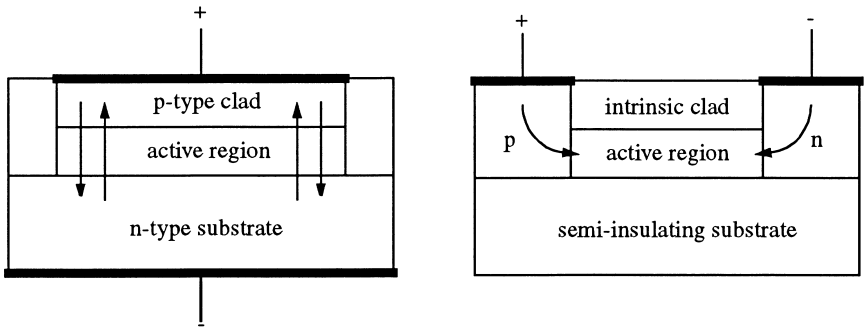

Fig. 1. Transverse cross-sections: (a) conventional vertical current injection laser; (b) lateral current injection laser.

1.2. Optoelectronic opportunities — integration and functional photonics

Integration in electronics provides a useful example for the field of optoelectronics. By the early 1960's, the electronics industry had encountered a bottleneck: the initial preoccupation with fabricating 'building block' devices was replaced with the need to connect these elements reliably and economically [6]. This demand was answered by the field-effect transistor: based on a predominantly *lateral* flow of current, this planar technology gave rise to the explosive and lucrative innovation of the monolithic integrated circuit.

Similarly, discrete optoelectronic components are capable of tremendous performance; however, electrical and optical interconnection of lasers, modulators, and driving circuitry is onerous. Integration not by extraordinary manipulations, but by controlled operations in the substrate plane, requires an intrinsically planar technology. In comparison, today's semiconductor lasers are intricately differentiated in the vertical direction, but are largely invariant laterally. As illustrated in Fig. 1(a), carrier injection is achieved through variations in doping in the vertical direction. Heavy doping exists throughout most of the structure.

The advent of *functional electronics* also provides valuable guidance for optoelectronics. Morton [7] pointed out in 1965 that electronic devices were dominated by mechanisms which gave rise to a simple, monotonic dependence of outputs on inputs. The simplicity of the equations which describe these relationships allows for representation using classical network equations.

Morton argued that much could be gained by exploiting the most basic interactions between energy and matter — that "...the aim of electronics should be not simply to reproduce physically the narrow elegance of classical circuit theory; rather, it should be to perform needed system functions as directly, as simply, and as economically as possible from the most relevant knowledge of energy-matter interactions" [9]. Morton's notion of functional devices is exemplified in electronics by the resonant tunnelling diode, in which internal quantum mechanical effects are evidenced in macroscopic device behaviour. Functional devices may replace large numbers of simple, interconnected devices with a small number of functionally sophisticated devices. Nature provides a direct solution to a problem which is more difficult to solve using less elegant methods.

1.3. Enabling planar optoelectronic integration

The vertical injection laser paradigm is incompatible with the goals of integration and functional device realization. In today's semiconductor lasers, the lateral direction is underexplored and largely inaccessible. Inertia is an important factor in this neglect. Currently available technology is a powerful determinant: tremendous precision and flexibility is available in the growth of complex vertical heterostructures. A compelling impetus is needed to induce those who design and fabricate semiconductor lasers to cast off their well-worn assumptions and methods.

If a fresh approach is to be taken, the assumption that injection of electrons and holes should be vertical must be set aside. Injecting current laterally (Fig. 1(b)) opens up a new spatial degree of freedom for exploration. If optoelectronic devices are fabricated by electrical and optical differentiation in the plane perpendicular to the direction of epitaxial growth, then devices with differing functionalities may be integrated monolithically without undue processing demands or performance compromises. Fabrication on an insulating substrate is an important advantage from the point of view of inter-device isolation. A single epitaxial structure compatible with both lasers and transistors may be used to form optoelectronic integrated circuits — aggregates of initially independent, then selectively interconnected, electronic and optical devices. Planar integration is compatible with microwave stripline interconnections on the surface of the substrate.

DFB: (longitudinal) Distributed Feedback laser
DBR: (vertical) Distributed Bragg Reflector

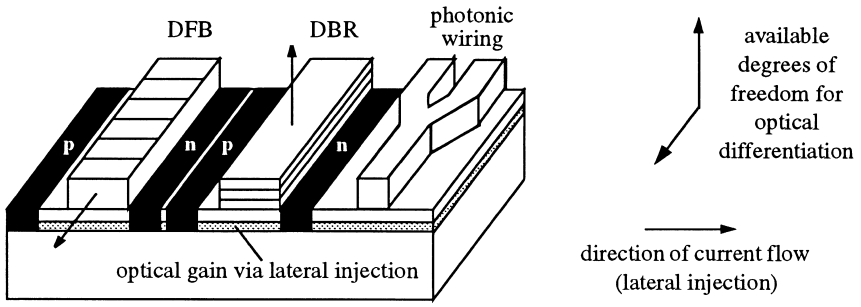

Fig. 2. Novel approach to photonic integration. With lateral injection, the vertical dimension is free for tailoring of optical properties. Instead of using semiconductor for vertical optical confinement, dielectric is be deposited and modified as required.

Ideally, photonic interconnections — analogous to the role played by wires in an electronic circuit — would be used to link monolithically integrated photonic devices. The lateral injection laser offers renewed opportunities for realizing this goal because it does not suffer from the constraint that the vertical cladding material participate in both optical confinement and carrier injection. Instead, dielectric optical waveguides could be deposited and modified following the elaboration of the electrical structure on the planar substrate.

A generic lateral injection p–n or p–i–n laser structure might be coupled (Fig. 2) with a resonant cavity to form a Fabry–Perot laser; a longitudinal grating to provide wavelength-selective feedback distributed along the length of the cavity (a distributed feedback, or DFB, laser); or a vertical distributed Bragg reflector (DBR) to form a surface-emitting laser. A longitudinal photodetector could be created by coupling light into a waveguide with an antireflection coated facet. These photonic devices, formed using the same basic electronic structure, would be connected using 'photonic wires', in analogy with electronic wiring.

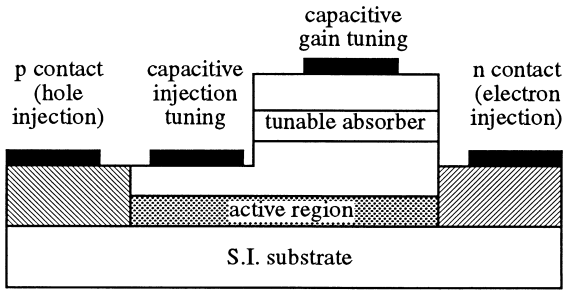

Fig. 3. (Transverse cross-section) Functional laser based on lateral injection of current. An electric field is applied capacitively to tune the lasing wavelength or modulate the injected current.

1.4. Enabling functional optoelectronics

Lateral injection offers new possibilities for the functional devices anticipated by Morton. A hybrid of a number of functional device ideas is illustrated in Fig. 3. Since lateral injection of current releases an additional spatial degree of freedom, the vertical dimension may be used for capacitive modulation of the gain in the active region while the lateral direction is used for current injection. Were capacitive modulation simply a mechanism for controlling the injection of carriers into the active region, it could be viewed as an elegant approach to integrating a laser with a transistor, in itself a desirable prospect. In fact, injection modulation is only one of a number of possibilities enabled by lateral injection. For example, the electronic properties of the active region may be modified by establishing an electric field across the active region, allowing the shape of the quantum wells and of their confined electronic states to be tailored. By modifying the optical gain spectrum in this manner, capacitive tuning of the lasing wavelength could be achieved.

1.5. Added advantages of lateral injection

The high parasitic capacitance of vertical lasers results from heavy doping throughout the epitaxial structure. This limits the speed of direct modulation. By decoupling the vertical and lateral directions, lateral current injection permits dopants to be added only at the level and locations required.

In the lateral injection paradigm, the vertical structure of a device may be designed so as to optimize confinement in that direction — for example, the vertical heterostructure may be chosen with a view to achieving a circular mode profile, or to devising quantum-confined electrical properties conducive to high-speed operation. Whereas in vertical injection it is

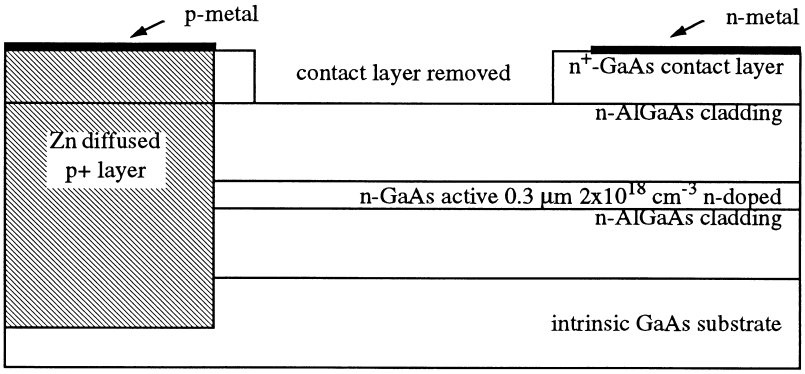

Fig. 4. The TJS structure grown on a semi-insulating substrate and reported in [13].

necessary to ease injection of carriers through this vertical heterostructure and to ensure that electrons and holes can meet and accumulate in relatively equal populations at all points, design of the electrical and optical structure is much less constrained once the lateral direction assumes primary responsibility for carrier injection.

In LCI lasers based on multi-quantum well active regions, increased differential gain and high modulation bandwidth may be obtained without compromising injection uniformity. Nonlinear modulation characteristics in vertical lasers result in large part from difficulty in injecting holes evenly into the different parts of the structure. It is thus advantageous to use the vertical structure for optical and electronic confinement and the lateral direction for smooth injection of electrons and holes parallel to the quantum wells.

2. Lateral injection lasers: 1974 to 1995

A number of groups of researchers, having been particularly enticed by the promise of monolithic optoelectronic integration, have sought to fabricate lateral lasers. A survey of these attempts is presented in this section. Experimental trials are grouped according to common structural features — the sequence of reports is therefore organized thematically rather than chronologically.

2.1. The transverse junction stripe (TJS) laser

2.1.1. TJS laser development at Mitsubishi

Namizaki, Susaki et al. pioneered the TJS laser and developed the device through a number of iterations [8–21]. Two basic structures were explored, the earlier grown on a doped substrate and employing a contact on either side of the substrate, the later grown on semi-insulating material and having both n- and p-contacts on the same side of the substrate (Fig. 4). The device depicted showed continuous-wave operation up to 100°C and room-temperature performance with a 27 mA threshold current and up to 15 mW output power per facet at 25°C.

2.1.2. TJS laser development outside of Mitsubishi

Kolbas et al. considered the role of Zn diffusion in intermixing the wells and barriers of a multi-quantum

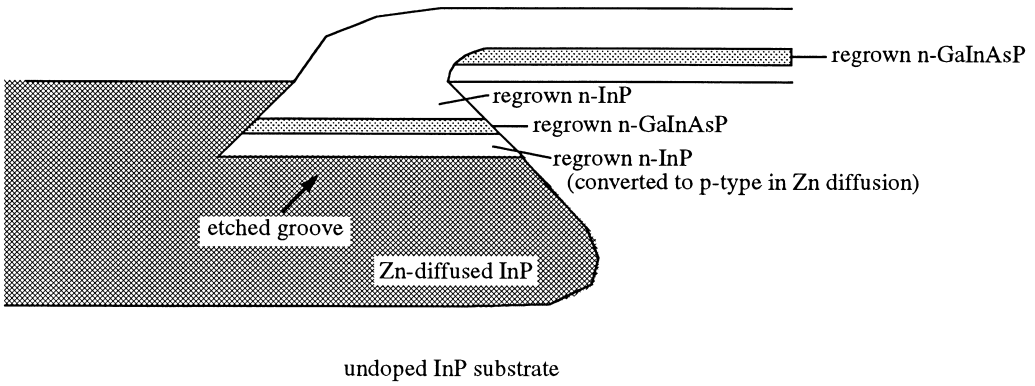

Fig. 5. Groove GaInAsP laser reported in [24,25].

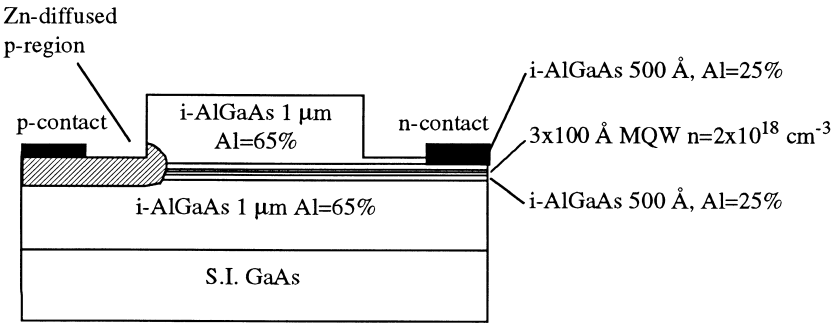

Fig. 6. The ridge-waveguide multi-quantum well transverse junction laser reported in [49].

well active region in order to introduce a lateral heterobarrier [22]; and studied experimentally the impact of surface leakage and parallel leakage in transverse junction lasers [23]. Yariv et al. applied the transverse junction approach to lasing in the GaInAsP materials system [24,25]. Devices were grown on semi-insulating material (an InP substrate in this case) and Zn was diffused in order to form a p-injector. In contrast to Mitsubishi efforts, vertical and lateral electrical confinement were achieved by growing the n-type GaInAsP active region inside a groove etched in the substrate (Fig. 5). Heavy doping was present in and near the active region and injection was predominantly vertical. The device exhibited continuous-wave operation up to 8 mW and pulsed-mode operation to greater than 200 mW/facet. At shorter wavelengths, 615 nm room-temperature continuous wave lasing was reported in an AlGaAs/InGaP TJS laser grown by liquid-phase epitaxy in 1992 [26,27]. The authors proposed that using a TJS structure rendered this device less vulnerable to poor interface quality between heteromaterials by reducing the effective junction area at the InGaP/AlGaAs interface.

2.1.3. Integrated and integrable structures

With a view to devising a planar process for TJS laser fabrication, devices were made by growing a TJS laser structure embedded in an etched semi-insulating GaAs substrate [28,29]. A monolithically integrated TJS laser and metal–semiconductor field-effect transistor were formed on a semi-insulating substrate [30–32]. In another effort aimed at achieving improved integrability [33–36], a structure resembling a traditional vertical-injection quantum well laser was used. The cladding material above the active region was doped p-type, the material below n-type. Two features were added: a junction field-effect transistor structure was integrated vertically with the active region; and both n- and p-contacts were formed on the top surface, the layers having been grown on semi-insulating GaAs. A similar effort was undertaken at AT&T Bell Laboratories [37,38]. With an eye to demonstrating photonic integration, Vawter et al. demonstrated integration with a low-loss optical waveguide [39]. A variety of further studies of TJS lasers have been reported relating to lineshape [40,41], a laser Doppler velocimeter [42], distributed feedback [43] (obviating the need for cleaved facets) [44] and surface emission [45–48].

2.1.4. TJS laser: advantages and limitations

The most successful TJS laser trials resulted in devices with competitive output characteristics which demonstrated the advantages of lateral current injection:

- compatibility with growth on semi-insulating material increased suitability for optoelectronic integration. Integrated laser-transistor and laser-waveguide structures were demonstrated;
- injection of carriers parallel to, rather than over, high-bandgap barriers allowed strong quantum confinement to be achieved without impeding injection;
- reduced injection area facilitated exploratory work in less mature materials systems;
- a transparent window above the active region facilitated grating-coupled surface emission.

Although TJS lasers exhibited good performance characteristics, enabled novel device explorations, and showed increased compatibility with optoelectronic integration, they suffered from some important limitations. In each of the devices considered, gain-guiding played an important role in confining the optical mode in the lateral direction. The gain and lateral mode distributions evolve with temperature and injection level. Gain-guided lasers have not achieved widespread acceptance because their output characteristics are not stable. A further concern in TJS lasers is that they permit only a limited decoupling of electrical and optical properties. In fabricating TJS lasers, the starting epitaxial material is strongly n-type throughout; the p-dopant is then diffused vertically through a portion of the wafer surface. When most or all of the material in and around the active region is heavily doped, the po-

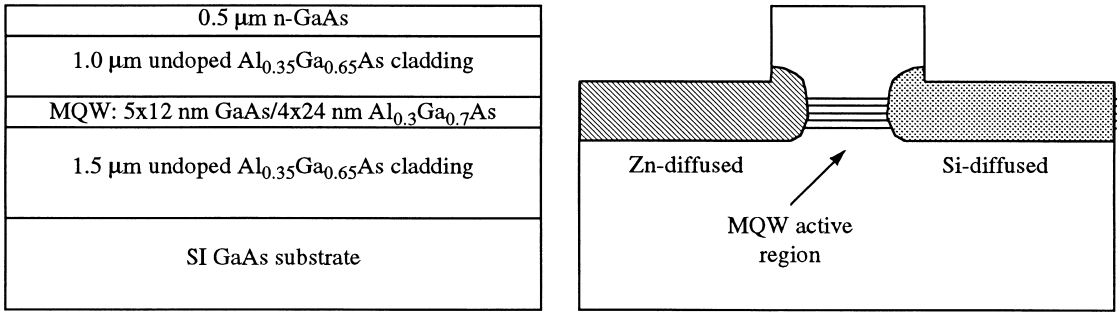

Fig. 7. Diffused-contact multi-quantum well laser reported in [50].

tential benefits of educed free-carrier absorption and chirp, lowered capacitance, and increased freedom to modulate laser characteristics capacitively are compromised.

2.2. The ridge-waveguide transverse junction laser

In view of the weaknesses of gain-guided lasers, most recent semiconductor lasers have employed index guiding. One TJS p–n junction device was reported by researchers at Minnesota and Honeywell [49]. The structure depicted in Fig. 6 exhibited 20 mA pulsed threshold current and a pulsed differential quantum efficiency of 12% per facet. This structure benefited from index-guiding via a ridge waveguide. Devices with ridges in the range 1–1.5 μm exhibited a stable single lateral mode.

2.3. Fujitsu p–i–n LCI laser

Wada et al. at Fujitsu [50–53] reported a series of p–i–n lateral injection lasers achieved by dopant diffusion. The epitaxial layers and the processed structure are illustrated in Fig. 7. Best results were obtained for a device with 0.5 μm wide ridge and active region. This device exhibited a room-temperature continuous-wave threshold current of 47 mA and differential quantum efficiency of 11%. In contrast, a 1.5 μm wide active region device exhibited an 800 mA pulsed threshold current. Room-temperature lasing was not obtained in wider devices. The authors attributed this strong dependence of threshold current on stripe width to the effect of heat produced by the driving current. They also speculated as to the possible impact of a laterally nonuniform carrier density distribution.

2.4. Electrotechnical laboratory regrown p–i–n laser

Suzuki et al. at Electrotechnical Laboratory in Japan reported lateral p–i–n lasers using sequential regrowth of high-bandgap, heavily-doped contact regions [54–57]. As seen in Fig. 8, two regrowths were required, one to form the n-contact, one for the p-contact. The resulting *L–I* characteristic shows a 35 mA threshold current for a device with a 1.5 μm wide active region. The wide-active region (4.5 μm) device exhibited a soft threshold characteristic and a rapid roll-off in efficiency above threshold. With refinements

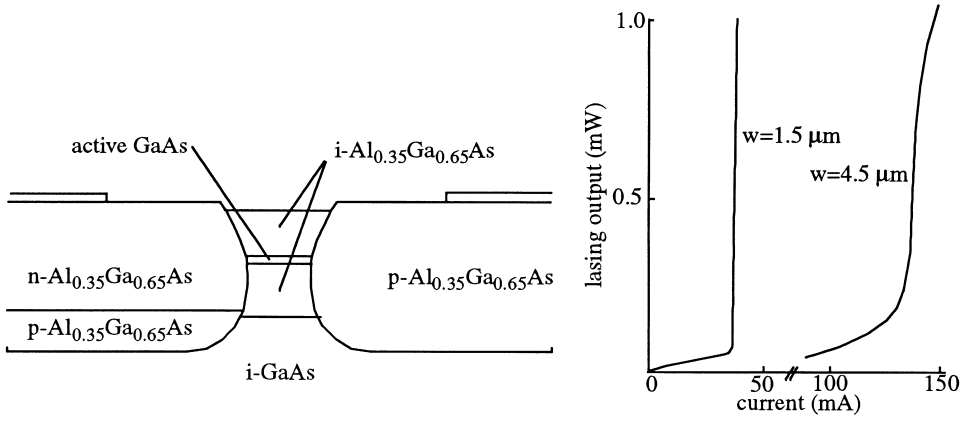

Fig. 8. Regrown-contact laser reported in [59].

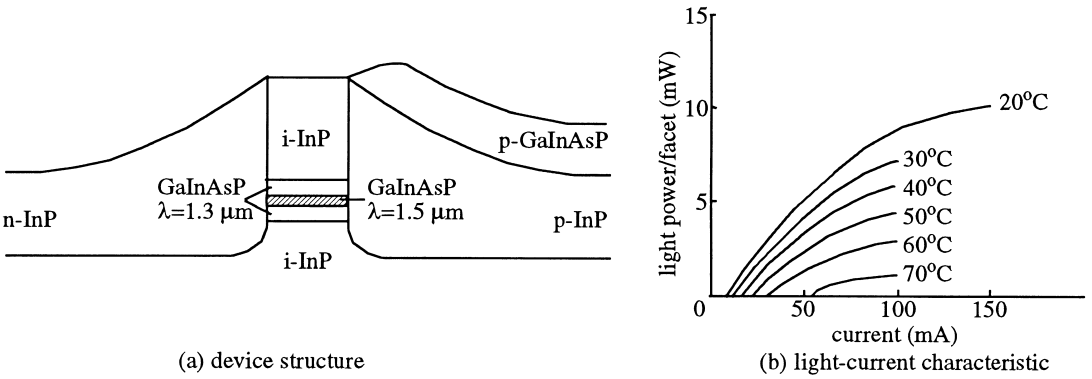

(a) device structure (b) light-current characteristic

Fig. 9. Doubly-regrown laser reported in [59].

in device processing, substantial improvements were obtained in device performance: a 1.5 μm wide active region device exhibited a 3.5 mA continuous-wave room-temperature threshold current and differential efficiency of 70% [55]. A similar device was reported in the InGaAs/InAlAs material system by another group [58]. While its performance was not as strong as devices in the more mature GaAs/AlGaAs system, this device embodied one of the advantages of lateral injection: the freedom to use high-bandgap InAlAs with a large conduction band offset in order to obtain large quantum effects without impeding carrier injection.

2.5. NTT/bellcore regrown p–i–n laser

A very successful LCI laser operating at 1.5 μm achieved via double-regrowth was reported in [59]. The structure, depicted in Fig. 9, consisted of 0.1 μm of bulk GaInAsP ($\lambda = 1.5\,\mu m$) with 0.25 μm of n-type GaInAsP ($\lambda = 1.5\,\mu m$) below and 0.25 μm of p-type GaInAsP ($\lambda = 1.5\,\mu m$) above. A 1 μm wide active region device operated in continuous-wave mode at room-temperature with a 10 mA threshold current and a maximum output power of more than 10 mW per facet.

2.6. Conclusions from literature survey 1974–1995

Empirical attempts at fabricating lateral injection lasers were not been without success: some of the devices performed well relative to their vertical injection counterparts.

On the other hand, many fabrication trials yielded devices whose performance was disappointing and unexplained. By 1995, after twenty years of exploratory lateral injection laser fabrication, no systematic attempt had been made at understanding the nature and importance of the physical mechanisms underlying the operation of the LCI laser. Nonuniform gain in these lasers is one example. Researchers at Fujitsu speculated that since p- and n-injectors are separated by a much greater distance in LCI lasers than in conventional vertical lasers, the lateral carrier density distribution may be nonuniform, and this may impede device performance. No quantitative estimate was given of the contact separation at which carrier density becomes significantly nonuniform. No clear relationship had been established to describe interactions between the optical mode and carrier density profiles. There existed no clear delineation as to the role of either gain nonuniformity or gain asymmetry in limiting performance, either below or above the lasing threshold.

Without a clear understanding of the importance of various mechanisms, the only method of designing improved devices would be one of trial-and-error. Without generalized, physically-motivated relationships between structure and performance, fabrication trials would provide little information as to the mechanisms at work. Little insight would be accrued, and little guidance would be made available for future reference.

3. Theory of the lateral current injection laser

In view of the limitations of the empirical approach of past efforts, a systematic investigation was initiated in 1995 in order to study the mechanisms which underlie the performance of the lateral current injection laser [60–67]. We summarize the results of these studies below.

3.1. Study of carrier density, gain, and optical modes

The distribution of carriers in the active region of a lateral current injection laser may be described with reference to ambipolar transport in the presence of a photon field. In determining the ambipolar profile of electrons and holes, it is necessary to take self-consistent account of:

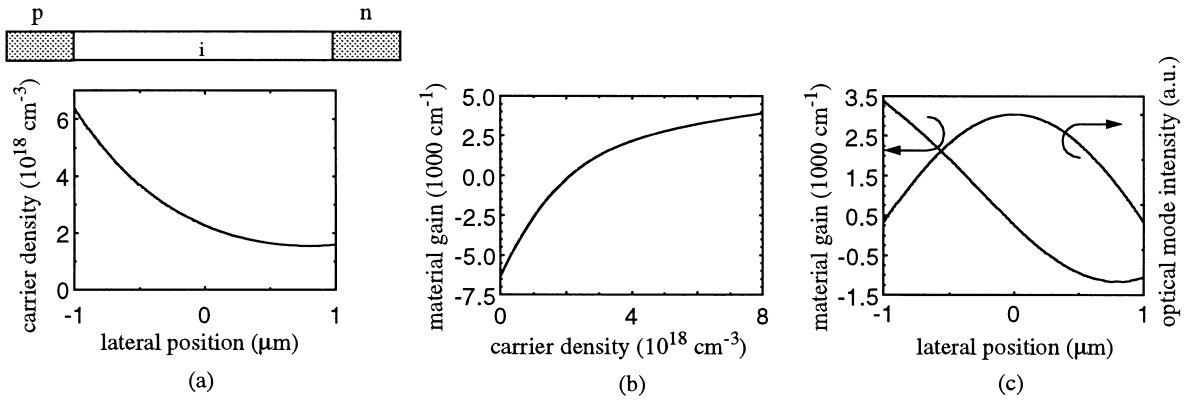

Fig. 10. (a) Lateral distribution of carriers (both electrons and holes under the assumption of $n \sim p$) in a p–i–n active region lateral injection laser. (a)– (c) combined suggest the relationship between carrier density, gain, and optical mode profile.

- those recombination mechanisms which are independent of a stimulating photon field: Shockley–Read–Hall, spontaneous and Auguer effects;
- stimulated recombination, which is dependent upon the local photon field density, as well as on the local gain (determined by the local carrier density);
- electron and hole drift and diffusion, Poisson's equation, and current continuity.

We have employed two contrasting approaches in developing the theory of the LCI laser:

- analytical model development, rooted in a number of approximations which serve to reveal key qualitative physical mechanisms;
- fully self-consistent, comprehensive 2-D modelling of specific laser transverse cross-sections, which, upon careful physical analysis, are also highly revealing and generalizable, and which also provide access to more subtle mechanisms.

In the approximation of quasi-charge neutrality (an excellent approximation in any laser within range of its threshold carrier density), an ambipolar diffusion-like equation may be obtained to describe the spatial profile of the carrier density, $n(x)$:

$$\frac{d^2n}{dx^2} = \frac{\mathscr{R}}{D} \tag{1}$$

where x is the spatial coordinate, $\mathscr{R}(x)$ the local recombination rate, and D is the ambipolar diffusion coefficient, related to the electron and hole diffusivities D_n and D_p according to $D = (D_n + bD_p)/(b+1)$where b is known as the electron–hole mobility ratio, defined as $b = \mu_n/\mu_p$.

If electrons and holes have similar mobilities ($b \approx 1$), the ambipolar diffusivity will equal their common diffusivity. If holes are much less mobile than electrons so that $b \gg 1$, then $D \approx 2D_p$, and the heavier carrier limits the ambipolar process. If electrons are much more mobile than holes, electrons flow to wherever they are needed to pair up with holes and satisfy quasi-charge neutrality; holes linger nearer to the point of injection. The characteristic diffusion of the less

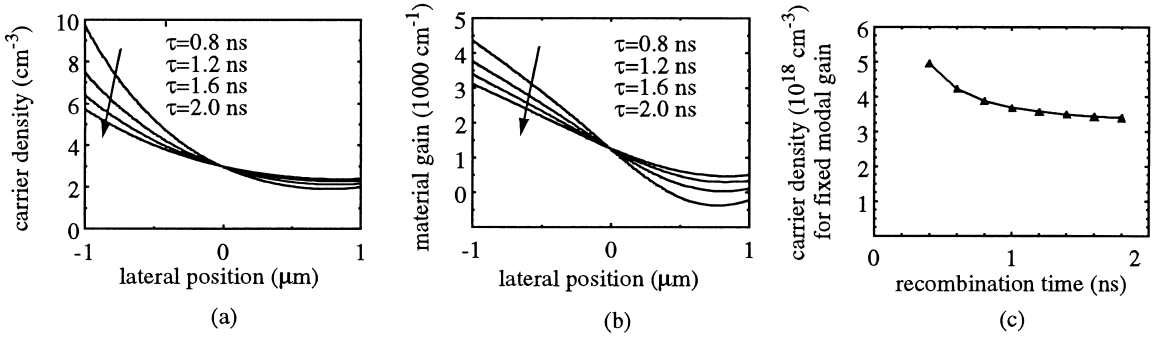

Fig. 11. (a) Carrier density across the intrinsic region for a fixed modal gain; (b) local material gain for fixed modal gain, calculated from (a); and (c) average carrier density across the active region required to achieve the same modal gain for different recombination times.

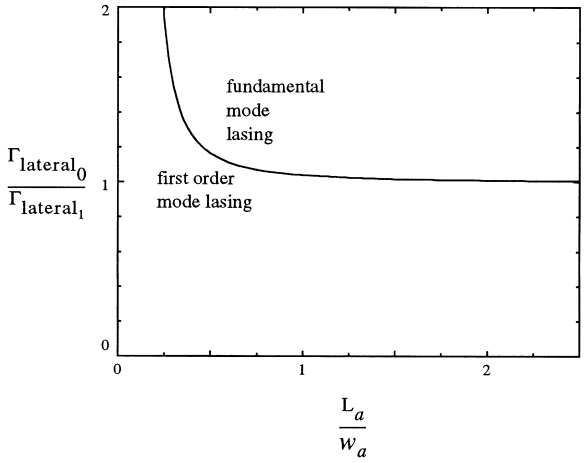

Fig. 12. Ratio of fundamental to first-order mode lateral confinement factor required for the two modes to experience the same net modal gain, plotted as a function of ambipolar diffusion length L_a normalized to active region width w_a.

mobile carrier determines the ambipolar carrier density profile.

In the further approximation of a constant recombination time τ — hence $R = n/\tau$ — solutions to (1) take the form $\cosh(x/L_a)$, $\sinh(x/L_a)$, where the ambipolar diffusion length is given by $L_a^2 = D\tau$. Current continuity at a given injection level fixes the coefficients of these two basis solutions.

The straightforward solutions which arise from such an initial approximate approach are already highly revealing. If the width of the active region — hence the separation of the electron and hole injectors — is much greater than the ambipolar diffusion length, the fundamental mode may be pumped inefficiently by the gain profile (Fig. 10). This situation deteriorates as the average recombination time decreases: mode-gain overlap worsens above the lasing threshold, providing one qualitative basis for above-threshold efficiency roll-off (Fig. 11). It is possible for the higher-order modes to lase first under conditions of severe carrier density nonuniformity (Fig. 12).

The issue of gain-mode overlap may be addressed very effectively in a number of ways:

- Lasers may be made with contact separations which are less than the ambipolar length. Present-day lithographic techniques are fully compatible with making active regions of widths less than a micron

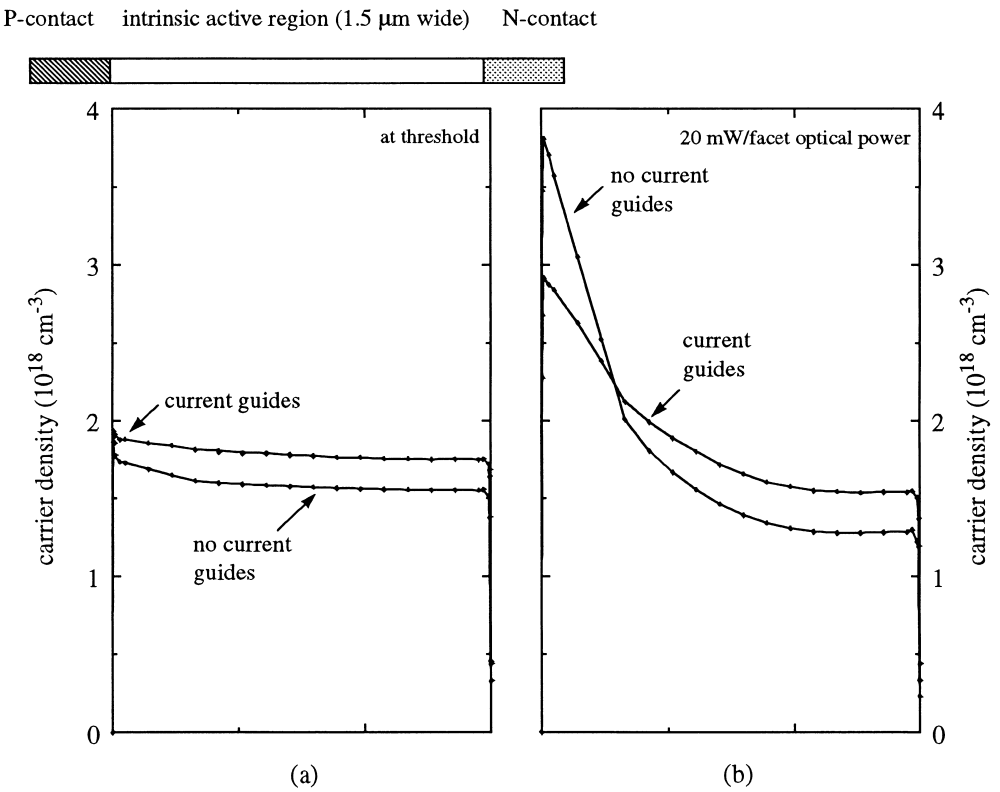

Fig. 13. (Simulation) Lateral carrier density profiles for lasers with and without current guides (a) threshold and (b) 20 mW/facet optical power.

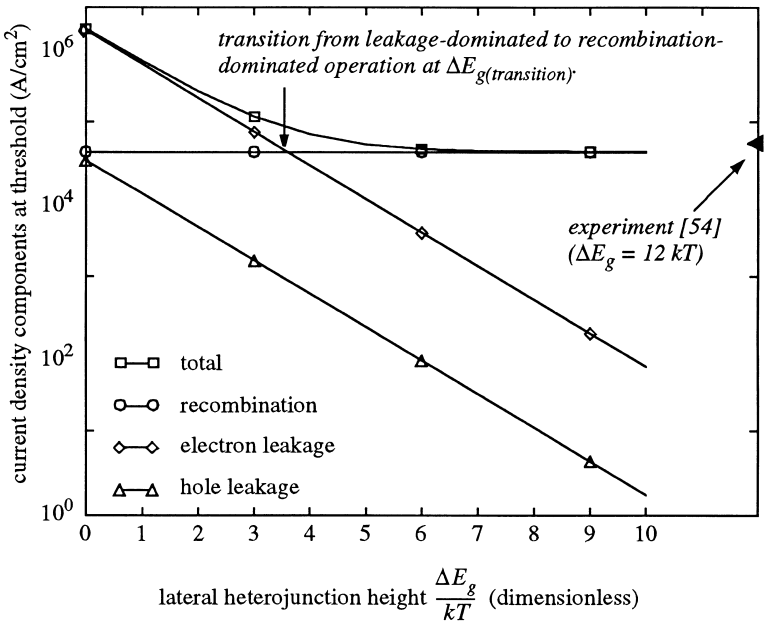

Fig. 14. Contribution of recombination and leakage to the total current density as a function of lateral heterojunction height for a lateral injection laser with a 1.5 μm wide by 0.3 μm thick active region.

— dimensions at which ambipolar effects are minimal even at moderate output powers.

- A large number of quantum wells may be used in order to keep the total confinement factor high, the threshold carrier density low, and superlinear recombination effects such as the Auger mechanism under control. The use of thick active regions is possible in LCI laser devices because injection occurs parallel to the wells. In LCI lasers with thick active regions, the far-field profile may be made essentially circular.
- Strained quantum wells may be used to admix the light-hole and heavy-hole wavefunctions, resulting in a reduced hole effective mass and increased hole mobility.
- By introducing current guides above and below the active region and by taking advantage of injection from the barriers, hybrid injection of carriers into the wells may be used to ensure a more uniform gain distribution (Fig. 13). We have explored this highly effect approach through modeling and experiment [70].

3.2. Heterojunctions and overbarrier leakage

Intuitive arguments might suggest that lateral carrier confinement should not be necessary in LCI lasers: if contacts are separated by a diffusion length or greater, carriers have ample chance to recombine radiatively before reaching the opposite contact. One might expect, on this basis, that efficiency would improve as the average carrier lifetime to decrease above the lasing threshold.

The fallacy in this argument rests in the fact that it does not take self-consistent account of the quasi-neutral distribution of electrons and holes. In fact, while the heavier holes will travel with difficulty across a wide active region, electrons will travel readily to the p-contact side of the active region. The electrons may then leak into the p-contact.

We have shown that lateral heterobarriers — even of modest height (e.g. as little as 4 kT) — are highly effective in confining carriers to the active region of a lateral current injection laser (Fig. 14). As discussed later in this work, the effectiveness of such modest heterobarriers implies that gentle, relatively noninvasive heterobarrier-forming methods — including selective quantum well intermixing — may be used to confine carriers to the active region.

3.3. Differential resistance and parallel leakage

By considering the aspect ratio of the width of the injection path to its length in lateral and vertical injection lasers, it may be imagined that the resistance in the lateral injection case will be greater. Previous authors were particularly concerned about resistive heating resulting from this effect.

We found that while resistive heating may certainly be an issue, the series differential resistance of the

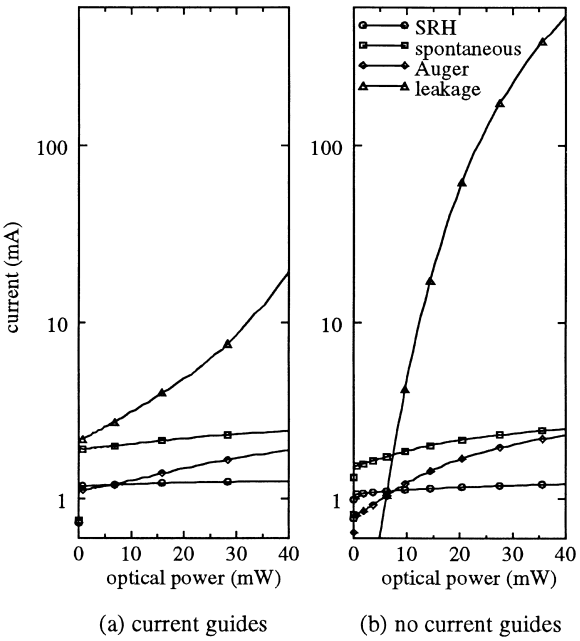

Fig. 15. Current components as a function of output optical power per facet for LCI lasers with and without current guides. While, as seen in Fig. 14, current guides are effective in reducing mode-gain overlap inefficiencies (reflected in the present figure in the slower rate of increase of parasitic currents above the lasing threshold), their most important quantitative impact in the case shown is to retard the onset of severe parallel leakage by lowering the series resistance of the active region.

active region is important in another respect. As voltage accumulates across the active region, it also grows across parasitic paths which are in parallel with the active region. Though the optical cladding material might have a much higher bandgap than the active region, it may nevertheless allow significant leakage under bias conditions required for passage of typical active region currents.

A number of solutions to the leakage issue are available. Increasing the ambipolar diffusion length, as discussed above, will lower the series differential resistance of the active region, as will the introduction of current guides and conductive barriers. Even entirely undoped current guides of intermediate composition may assist in hybrid injection and lead to a reduction in differential resistance (Fig. 15). Maximizing the doping of the injectors near the heterojunction will contribute to a lowering of the differential resistance of the heterojunction itself. Finally, high-bandgap cladding material, highly resistive cladding material, or any available blocking mechanism (e.g. oxidation, pnpn blocking layers) will keep parallel leakage under control at optical powers of interest.

4. LCI laser fabrication: opportunities and challenges

With the theory of the lateral current injection laser operation having been developed and its consequences explored, two important further challenges remained:

- to tailor technologies for the fabrication of lateral injection lasers in particular and for the development of monolithic optoelectronic integrated circuits and novel functional devices in general;
- to deploy a selection of such processes in the realization of devices which would allow combined experimental–theoretical investigations of operating mechanisms of lateral injection devices.

We illustrate in Fig. 16 the two fabrication paths which we have followed, and which determined the focus of our fabrication process research. An approach based on ion implantation and annealing for selective-area doping and heterobarrier formation is illustrated in Fig. 16(a). This approach lends itself to widespread use as a planar fabrication technology, and is in fact already well established in the fabrication of electronic devices. Its potential for enabling practical monolithic integration is readily apparent.

An alternative approach, this one based on the removal of active region material in the contact area, followed by regrowth of a heavily-doped, high-bandgap material in its stead, is depicted in Fig. 16(b). The great promise of this technique lies in its potential to create high-quality, high-mobility, heavily-doped, large-bandgap material for low-resistance injection and strong carrier confinement.

Since LCI laser fabrication builds substantially on the familiar platform used in realizing vertical injection lasers, we focus on those processes which are novel to the lateral injection case, or which require further tailoring relative to existing vertical injection laser fabrication techniques.

4.1. Smooth, low-damage dry etching

The following results were desired of the etch processes depicted in Fig. 16:

- nearly vertical sidewalls;
- low-damage etching, especially near to the active region;
- a reasonably fast etch rate, a micron or more of material needed to be etched.

While chlorine-based dry etch chemistries are often used in the processing of GaAs and related materials, these typically result in rough surface morphologies in the InP system. This is attributed to the difficulty in achieving volatilization of $InCl_3$ under readily accessible temperature and pressure conditions [71]. Chemistries based on the use of methane and ethane

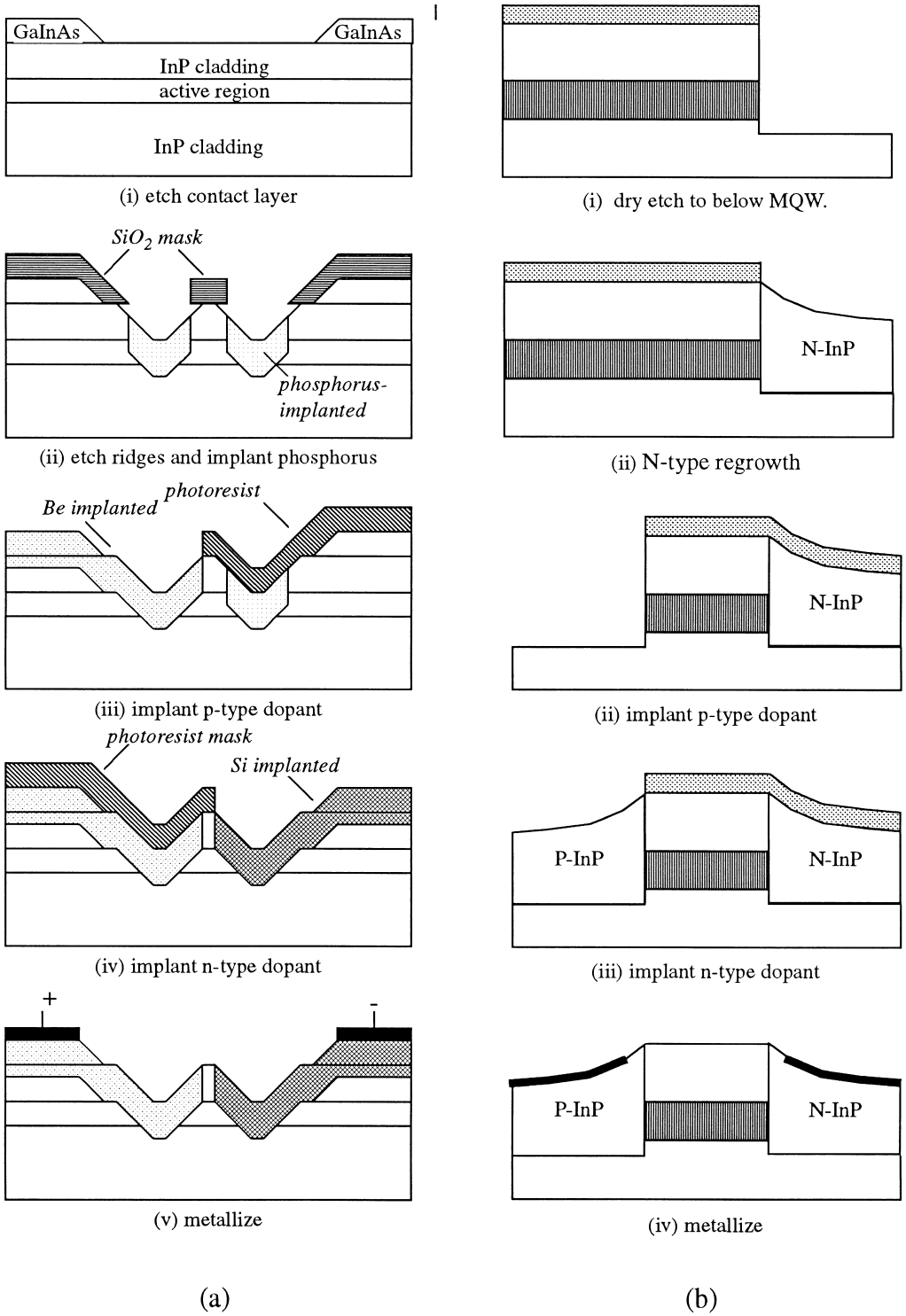

Fig. 16. Typical process sequences for (a) ion implantation doped and intermixed LCI laser; (b) etched-and-regrown LCI laser.

are reported to give rise to smooth etch morphologies in the InP system. Collisions between energetic plasma molecules and the semiconductor surface can create surface and subsurface damage. Pearton [72] assessed these effects experimentally, finding that an ethane-based RIE gave rise to damage as follows:

- a highly disordered, nonstoichiometric (indium-rich) region between the surface and 150 Å depth;
- a stoichiometric but significantly disordered layer between 150 and 400 Å;
- point defects to a depth of about 1000 Å, producing some degree of carrier compensation but no disruption to the crystalline order as detected using ion channeling analysis.

Significant damage created during RIE of InP motivates explorations of techniques which rely on less kinetic (lower self-bias) approaches. The electron cyclotron resonance method is advantageous from this point of view: the energies of ions reaching the sample are typically less than 15 eV, less than the displacement threshold for damage in InP [76].

We implemented a relatively new approach to etching InP recently reported [73]. A Cl_2/N_2 mixture is used in an electron–cyclotron resonance system, allowing a vertical profile and smooth etched surface to be achieved using a low-energy (about 30 eV) ECR plasma for minimal damage. The improved smoothness of this etch relative to the Cl_2/H_2 system was attributed to (a) a reduction in the density of chlorine radicals by dilution with an inert species (N_2); and (b) the formation of a nonvolatile P_3N_5 species which helps in equalizing the In- and P-based product desorption rates. We obtained smooth etching and vertical profiles using this lower-energy bombardment method.

4.2. Doping via ion implantation

Ion implantation is extensively used in electronics, particularly in the fabrication of field-effect transistors. Among the desirable features of ion implantation are [74]:

- the reproducibility of the doping process and its lack of dependence on surface preparation;
- the simplicity of dose control by current integration;
- the simplicity of masking techniques, including the option of using only photoresist;
- the possibility of implanting through passivation layers such as SiO_2;
- the relative freedom in the choice of doping profile via the use of multiple-energy implants.

The decomposition of InP above 360°C [75] presents a significant challenge. Surface decomposition results in the formation of pits on the surface of the sample, resulting in increased optical scattering. Changes in surface composition are often accompanied by the production of an n-type layer [76], impeding p-type activation and contact formation. Techniques for the protection of the semiconductor surface have been developed in response. Annealing may be performed in the proximity geometry [77], wherein the sample is placed in direct contact with another wafer in order to create a local group-V overpressure. The proximity geometry has been reported to preserve a high surface quality during at maximum annealing temperatures varying between 700°C [78] and 750°C [79]. The use of a graphite susceptor containing granulated InP and the execution of a capless rapid thermal anneal in a PH_3/H_2 atmosphere [79] have also been shown to aid in preserving surface integrity. Another method involves the use of a dielectric cap such as Si_3N_4. Degradation-free anneals to 900°C have been reported using a combination of methods. One concern over the use of the Si_3N_4 cap is in-diffusion of Si which results in unintentional n-type doping of the surface layer [76].

Activation of acceptor implants is another challenging task. Peak hole concentrations are generally limited to $1–2 \times 10^{18}$ cm^{-3}. During annealing, impurities near the semiconductor surface may leave the sample entirely. Beryllium, among the most commonly used p-type dopants in then InP–GaInAsP system, is particularly diffusive. The interstitial–substitutional mechanism by which it diffuses [79] is dependent upon the concentration of acceptors and vacancies in the group III sublattice. Since indium and phosphorus have substantially different masses, implantation tends to result in an accumulation of In (the heavier element) near the surface and P (the lighter element) at greater depths [80]. At the surface, where group III vacancies are scarce, beryllium does not activate well and instead diffuses downward to where there are more group III vacancies. Heckingbottom and Ambridge [81] addressed this problem by implanting a group V element along with the Be to balance out the excess In at the surface and provide a group V overpressure. The more even stoichiometry at the surface improved electrical activation and suppressed in-diffusion.

4.3. Selective formation of heterobarriers via quantum well intermixing

Quantum well intermixing refers to the interdiffusion of materials in a heterostructure at elevated temperatures. In the limit of strong intermixing, a complete alloying of adjacent layers may be obtainable. While intermixing will eventually occur if a heterostructure is heated to a sufficiently high temperature, it is of practical utility if achieved selectively. A number of methods for enhancing intermixing have been reported:

- deposition of a dielectric layer above the region to

be intermixed [82];
- diffusion of an impurity, typically a dopant such as Si or Zn [83];
- implantation neutral or dopant ions into the region to be intermixed [84,85].

Implantation of neutral impurities directly into the material to be intermixed has been studied in the GaInAsP/InP system. 100 keV phosphorus ions were implanted with doses between 1×10^{14} and 1×10^{15} cm^{-2} into a structure with a single 75 Å GaInAs well clad by InP. Photoluminescence shifts of 200 meV were obtained from a starting wavelength of 1500 nm [84]. Annealing was carried out either at 650°C for 30 min or in an a rapid thermal annealing (RTA) system at 750°C for between 5 and 40 s. Waveguide losses were found to be as low as 3.5 cm^{-1} at 1550 nm. Another series of experiments [86] in which only small blueshifts were obtained (up to 35 meV in 55 Å quantum wells) revealed significant differences in blueshift between structures in which the wells were compressively-strained (greatest shift), tensile-strained (least shift), and unstrained (intermediate shift). These results were attributed to differences in composition in the differently-strained materials. The same group later obtained shifts as large as 240 meV using 30 Å compressively-strained GaInAs wells clad by InP [87]. In studying the relationship between anneal temperature and the formation of pits on the surface of samples, the authors found that annealing at 700°C for 13 s resulted in maximum intermixing without noticeable surface degradation. It was found that beyond a certain dose, the degree of intermixing started to decrease with increasing dose. This effect was attributed to the formation of complex defects which can capture migrating simple defects and reduce the total number of defects which cross the interface between well and barrier [87].

Lateral spatial resolution is connected with the lateral straggle of ions during implantation and with the lateral diffusion of impurities and vacancies through the material. In one experimental report, presumably with both of these effects carefully under control, buried GaInAs/InP quantum wires with dimensions below 100 nm [88] were formed using intermixing resulting from implantation into quantum wells.

4.4. Selective area regrowth

The desirability of buried-heterostructure vertical injection lasers with simultaneous electrical confinement, current blocking, and optical confinement motivated much of the early work on regrowth [89]. The rate and morphology of epitaxial growth depends on the surface on which material is to be deposited. Dielectric material is often used to mask selected areas, leaving some semiconductor material exposed. If polycrystalline material is deposited on the dielectric while monocrystalline growth occurs on the semiconductor in the open windows, the result is known as phase-selective growth. In true selective-area growth, the growth rate vanishes on the mask material.

The mechanism which gives rise to selectivity during MOCVD is related to desorption and gas phase diffusion during growth [90]: molecules deposited on the mask desorb, collide with molecules in the gas phase, return to the mask surface, and stick only if they strike openings in the mask. The pressure in the reactor is one determinant of the communication distance, or migration length, which a species can move along the mask toward an available opening. The communication distance and the selectivity may be increased by decreasing pressure, using reagents with low partial pressures, and increasing the growth temperature. In addition, since the elemental species (e.g. Ga, In) exhibit higher sticking coefficients than the metallorganic precursors, selectivity is enhanced if the incoming reagents are not fully decomposed before reaching the surface of the substrate. MBE is essentially a phase-selective technique for this reason.

If a high degree of selectivity is achieved, reagents are consumed exclusively in the mask openings. A lateral concentration gradient parallel to the wafer surface results, and the growth rate in the stripe openings is enhanced relative to the case of an unmasked substrate. The nature of the exposed crystal planes also influences regrowth morphology. Different exposed crystallographic surfaces exhibit different numbers of free bonds per atom. This influences their chemical reactivity during wet etching and, for similar reasons, affects their propensity to promote nucleation during epitaxy [91].

A regrown interface of poor quality may give rise to a high surface recombination velocity. Frei et al. [92] studied this effect by measuring the ideality factors of p–n heterojunction diodes fabricated using regrowth. If the GaInAs on which regrowth was carried out was etched using a 5:1:1: H_2SO_4:H_2O_2:H_2O solution immediately prior to regrowth, the performance of the diodes was indistinguishable from that of devices fabricated by continuous growth, indicating that high-quality interfaces were obtained. In studying the effect of a variety of surface preparations prior to overgrowth on GaInAs, Yablonovitch et al. [93] obtained best results by etching in hydrobromic acid solution and rinsing in concentrated sulfuric acid immediately prior to regrowth. The authors estimated the resulting surface recombination velocity to be less than 20 cm/s. The next-best surface pretreatment was to use the solution H_2SO_4:H_2O_2:H_2O 1:8:5000 immediately prior to etching; this resulted in an estimated surface recombination velocity of 50 cm/s.

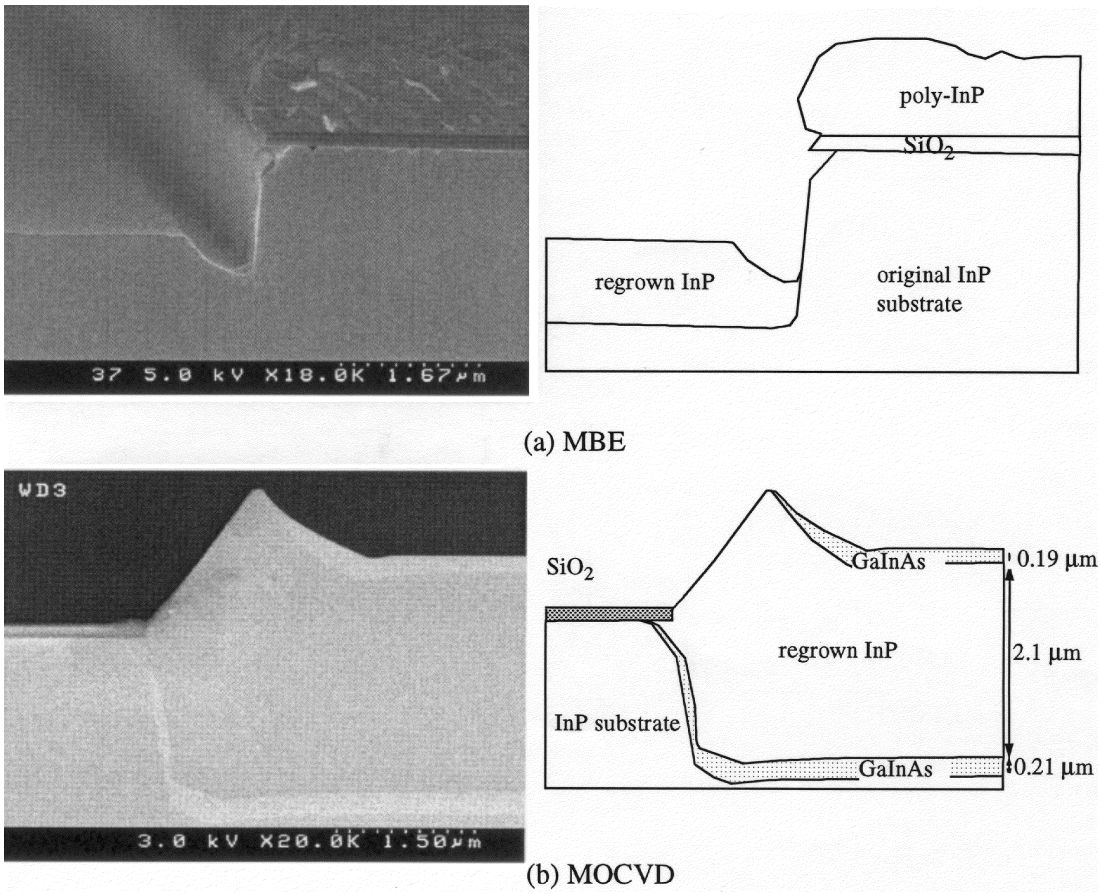

Fig. 17. (a) FE-SEM image and labelled trace showing the result of MBE overgrowth on a bulk InP substrate; (b) of MOCVD-overgrown InP.

We characterized both MBE and MOCVD selective-area growth in the context of our materials system. MBE regrowth was performed on a bulk InP wafer in order to study the rate and morphology of regrowth using this technique. The sample wafer was prepared by depositing SiO_2, patterning the wafer lithographically, transferring the pattern to the SiO_2 using a CHF_3 etch, and dry and wet etching using the technique developed and described above. The result of this process is illustrated in Fig. 17(a). As is characteristic of MBE overgrowth, polycrystalline InP was deposited atop the SiO_2 mask. The regrown material was observed to exhibit one potentially troublesome morphological feature apparent in the figure: the single-crystal InP exhibited a reduction in growth rate of about a factor of two near the mask edges. Far from this interface, the growth rate was the same as on a full, unpatterned wafer. An atomic force microscope was used to acquire two-dimensional profiles of the surface of the regrown material. The surface roughness was found to be on the order of 30 nm; since this value is an order of magnitude less than the wavelength of light in the medium, it was believed to be acceptable for this application.

MOCVD regrowth was also studied. Since half of the wafer area was masked with SiO_2, it was expected that substantial growth rate enhancement would be observed. N-doped 1×10^{18} cm^{-3} layers were grown as follows: 0.1 µm GaInAs; 1.0 µm InP; 0.1 µm GaInAs. The bottom GaInAs layer was to serve as a marker. Far from the mask edge, the growth rate relative to the case of an unpatterned wafer was doubled (Fig. 17(b)); closer to the edge, the results of a further increase in rate could be seen. These so-called 'rabbit ears', while an undesired morphological feature, were not expected to affect device performance significantly in this application. (They can impede lithographic alignment in later steps, however.) It is interesting to note that the first ternary marker layer grew on the nearly vertical sidewalls.

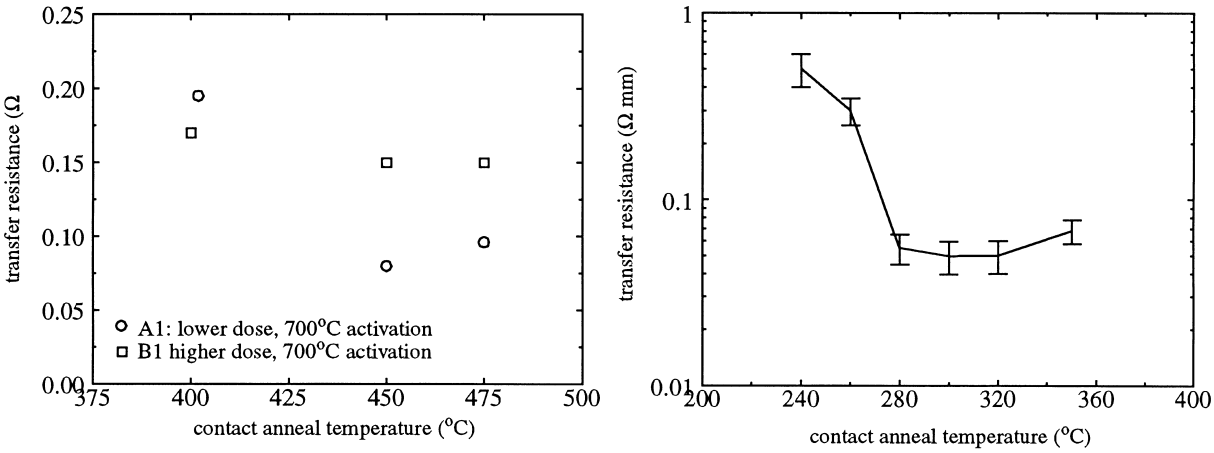

Fig. 18. (a) Transfer resistance versus contact anneal temperature for Be-implanted structures annealed at 700°C for 10 s and at variable temperatures for 30 s following e-gun evaporation of 500 Å Ti; 750 Å Pt; 2000 Å Au. (b) Transfer resistance versus contact anneal temperature for Si-implanted structures annealed at 700°C for 10 s and at variable temperatures for 1 min following e-gun evaporation of 25 Å Ni; 800 Å Au; 400 Å Ge; 600 Å Au.

4.5. Ohmic contacts to GaInAsP

Ohmic contacts should have negligible contact resistance relative to the series resistance of the semiconductor device of which they form a part. Practical metalizations usually result in Schottky contacts, wherein an energetic barrier impedes the flow of current between the metal and the semiconductor. If the barrier is low enough, thermionic emission over the barrier may be possible. Even if the barrier is high relative to the thermal energy of a typical electron, it is possible in heavily doped semiconductors for the depletion region to so thin as to admit electron tunneling. Such contacts may exhibit low-resistance, linear or quasi-linear I–V characteristics over the range of interest, in which case they are often thought of for practical purposes as ohmic contacts.

Low-resistance contact formation is aided by the introduction of a high level of doping of the appropriate type into the semiconductor layer to which contact is to be made. A number of approaches may be taken in order to achieve a high level of surface doping [94]:

- heavy doping during epitaxial growth;
- diffusion or ion implantation of a dopant species;
- alloying and subsequent recrystallization with a set of evaporated metal layers of which one is a donor or acceptor in the semiconductor. For example, in making contacts to p-type III–V materials, Zn and Be dope the surface region of the substrate during annealing, resulting in an enhancement of tunneling current and giving rise to ohmic behaviour [95].

A more complex situation arises when it is sought to make ohmic contacts to semiconductor heterostructures. Large, abrupt changes of doping or composition within the semiconductor give rise to the formation of internal barriers to current flow. Alloying between the metal and semiconductor may aid in lowering internal barriers. In addition to smoothing out the doping profile, this alloying process may give rise to intermixing of the heterostructure [96], a phenomenon noted in the study of the formation of contacts to a two-dimensional electron gas inside and a HEMT.

In the GaInAsP/InP material system, low-resistance ohmic contacts are most readily formed on GaInAs, since this provides the lowest energetic barrier and highest achievable doping level. One common metallization is the Au–Ge–Ni alloy system. The thin layer of nickel which is deposited first is used to promote adhesion between metal and semiconductor. Germanium serves as an n-type dopant once it diffuses into the semiconductor material during contact annealing [96]. For p-type contact formation, alloyed Au–Be and Au–Zn metallizations are frequently used since Zn and Be serve as p-type dopants [97].

We studied the formation of low-resistance contacts to GaInAs which is originally nominally undoped, and which is then heavily doped p- or n-type via ion implantation followed by rapid thermal annealing. We grew a nonintentionally doped $Ga_{0.47}In_{0.53}As$ layer ($n = 1 \times 10^{15}cm^{-3}$) on top of 0.5 μm nonintentionally doped InP grown by MOCVD on (100) oriented semi-insulating InP:Fe. Beryllium was implanted in a non-channeling 7° direction according to the schedule indicated in. For contact to p-implanted material, the following layers were evaporated using the e-gun technique at a base pressure of 1.4×10^{-6} Torr: 500 Å Ti; 750 Å Pt; 2000 Å Au. After lift-off the samples were sintered at temperatures of 400, 450 and 475°C for 30 s in an N_2 ambient. The quality of the surface of

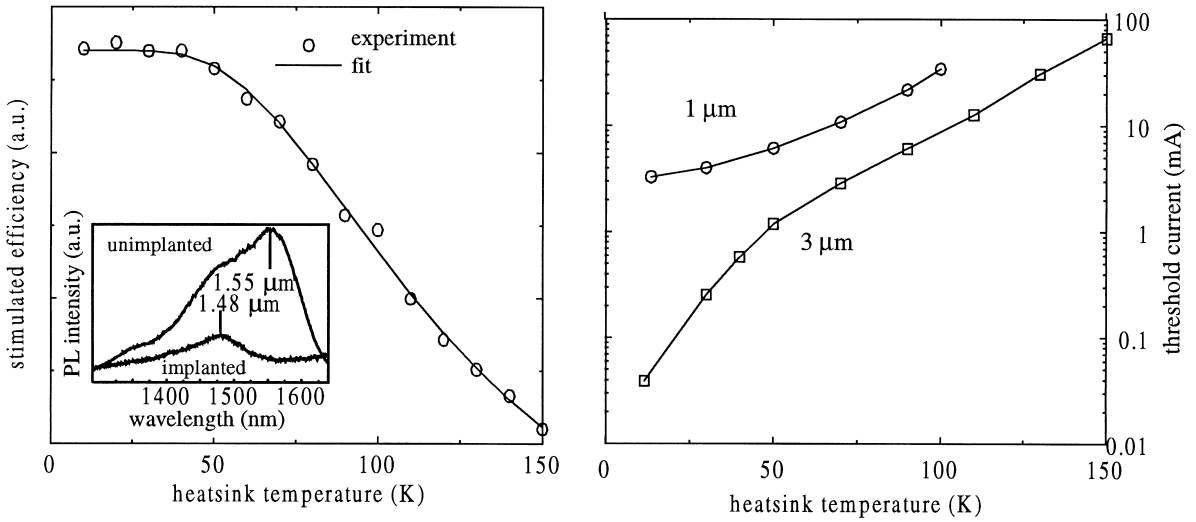

Fig. 19. (a) Stimulated efficiency vs. heatsink temperature for a device with a 3 μm wide ridge; (b) threshold current vs. heatsink temperature for 1 and 3 μm ridge devices.

annealed samples was found to depend on implanted dose and anneal temperature. The surface of the lower-dose samples was free of obvious pitting after the 700°C anneal, but showed the onset of pit formation at 750°C. In contrast, the higher-dose sample showed some degradation in surface morphology even after the 700°C anneal. The best contacts exhibited a transfer resistance 0.08 Ωmm; these were produced on the lower dose sample (A) by annealing at 700°C and sintering at 450°C. Contacts to samples annealed at 750°C were ohmic, but showed a high resistance attributed to the surface damage. The higher dose sample annealed at 700°C exhibited a higher minimum transfer resistance than the lower dose sample, and a reduced temperature sensitivity in its transfer resistance.

We also studied the formation of contacts to nonintentionally doped $Ga_{0.47}In_{0.53}As$ layer ($n = 1 \times 10^{15}cm^{-3}$) on top of 0.5 μm nonintentionally doped InP into which Si was selectively implanted in a nonchanneling 7° direction using a patterned 1.2 μm thick photoresist mask. The e-gun technique was used to evaporate at a base pressure of 5×10^{-6} Torr the following layers: 25 Å Ni; 800 Å Au; 400 Å Ge; 600 Å Au. The 25 Å bottom Ni layer was used to improve adhesion to the semiconductor. After lift-off the samples were placed between a pair of Si wafers and rapid thermally annealed at temperatures ranging between 240°C and 450°C for 60 s in an N_2 ambient. Whereas samples annealed at 700°C showed a clean surface morphology following the implantation anneal, samples annealed at higher temperatures showed a high density of pits. A plot of contact transfer resistance in Ω mm versus contact anneal temperature is given in Fig. 18(b) for samples whose Si implants were annealed at 700°C. Contacts to the pitted samples which were annealed at 750 and 800°C exhibited much higher contact resistances. To within the uncertainty of the transfer resistance measurement technique, it would appear that there is a broad annealing temperature range (280 to 320°C) over which ohmic contacts with transfer resistances of 0.05 Ωmm may be achieved. The transfer length obtained was used to calculate a specific contact resistance of 7×10^{-7} Ω cm^2. For comparison, a previous report of contacting to ion implantation doped n-type $Ga_{0.47}In_{0.53}As$ yielded a minimum specific contact resistance of 1.5×10^{-6} Ω cm^2 [98]. For a lateral current injection laser of length 300 μm, the preceding results would imply that a metal–semiconductor contact resistance of less than 0.2 Ω may be achieved.

5. Experimental explorations of LCI laser operation

5.1. Ion implanted quantum-well intermixed LCI laser [68]

The process depicted in Fig. 16(a) was executed in order to facilitate study of the physical effects discussed in Section 3 and the processing technologies of Section 4. The epitaxial structure was grown by organo-metallic vapor phase epitaxy on InP:Fe. The bottom cladding consisted of 1 μm InP:Fe. The active region, with photoluminescence peak at 1.55 μm, was made up of ten 95 Å 1% compressively strained undoped wells separated by 190 Å 0.5% tensile strained $Ga_{0.18}In_{0.82}As_{0.25}P_{0.75}$ ($Q = 1.1$ μm) p-type

5×10^{17} cm^{-3} barriers. Above and below this multi-quantum well (MQW) structure were 500 Å thick layers of unstrained GaInAsP ($Q = 1.07$ μm) doped p-type 5×10^{17} and 1×10^{18} cm^{-3}, respectively. The top cladding consisted of 0.5 μm undoped InP, on top of which was grown a 0.2 μm thick contact layer of undoped $Ga_{0.47}In_{0.53}As$. Iron doping was used in the substrate and lower cladding to reduce parallel leakage current. Compressively strained quantum wells were used to minimize Auger recombination and break the heavy hole–light hole degeneracy, thereby reducing the heavy hole effective mass and increasing the hole mobility. Current guiding layers above and below the MQW, along with the thick p-doped barriers, served to reduce the series resistance of the active region by promoting hybrid injection of holes.

The resulting devices permitted study of the physical mechanisms which underlie LCI laser operation. Shown in Fig. 19(a) is the measured evolution of the stimulated emission efficiency as a function of heatsink temperature. By fitting to a model of stimulated efficiency which accounts for the temperature dependence of the various recombination mechanisms and of leakage over the heterobarriers, we estimated the degree of lateral heterobarrier formation obtained by implanting and annealing to have been around 30 meV. This agrees with the measured room-temperature photoluminescence spectral shift of 38 meV for implanted versus unimplanted materials annealed under the same conditions (inset of Fig. 19(a)).

Shown in Fig. 19(b) is the temperature dependence of threshold current for lasers with 3 and 1 μm wide ridges. The fact that the threshold current is appreciably lower for the wider-ridge devices would suggest that the 1 μm wide device experiences a larger scattering loss. There is a discontinuous change in the slope of the threshold current temperature dependence for the 3 μm wide device around 50 K; this coincides with a change in the far field from first-order transverse mode lasing below 50 K to fundamental mode lasing above this temperature. This observation, and the lack of an analogous discontinuity in the case of the 1 μm wide laser, is explained with reference to the laterally nonuniform carrier density distribution [68]. The decreased low-temperature mobility arising due to increased ionized impurity scattering below ~50 K gives rise to a reduced ambipolar diffusion length. This enables first-order mode lasing in the 3 μm wide ridge device prior to fundamental mode lasing. In the 1 μm wide ridge device, there is no first-order lateral mode admitted (or its confinement factor is very small), so lasing always occurs first on the fundamental mode. However, as the ambipolar diffusion length drops at low temperatures, the threshold current drops more slowly as gain-mode overlap worsens with increasing lateral carrier density nonuniformity.

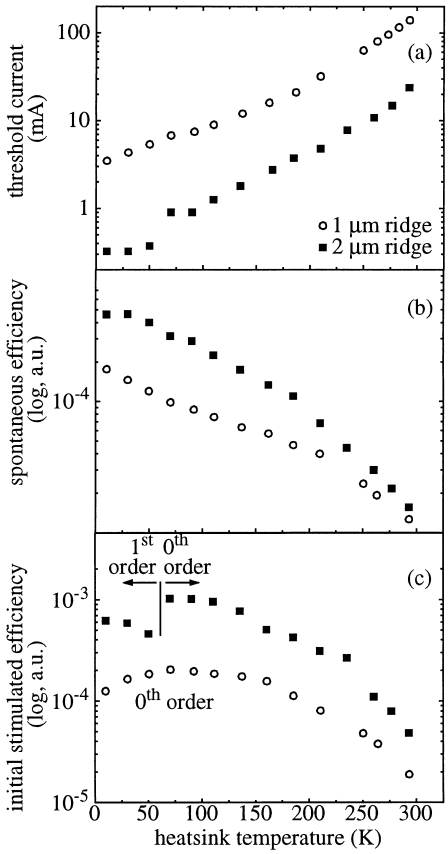

Fig. 20. Comparison of temperature evolution of measured (a) threshold current, (b) spontaneous efficiency and (c) stimulated efficiency with heatsink temperature under 1 μs/0.1% pulsed excitation in 1 and 2 μm wide active region devices

In this experimental study, two key features of lateral current injection lasers were revealed. The relationship between stimulated efficiency and lateral heterobarrier formation was demonstrated, and it was found that a large but realizable bandgap shift achievable by ion mixing should enable room-temperature LCI laser operation. The relationship between ambipolar diffusion length and lateral optical mode profiles, another key feature in LCI lasers, was also demonstrated experimentally.

5.2. Etched, regrown and diffused LCI laser [69]

The process depicted in Fig. 16(b) was carried out with one slight modification: instead of two separate regrowths, a single etch and regrowth was carried out, and was followed by selective Zn diffusion in order to turn one InP contact p-type. The epitaxial structure used in this investigation was grown on Fe:InP via low-pressure metal organic chemical vapour deposition. Ten 55 Å undoped 1.5% compressively strained

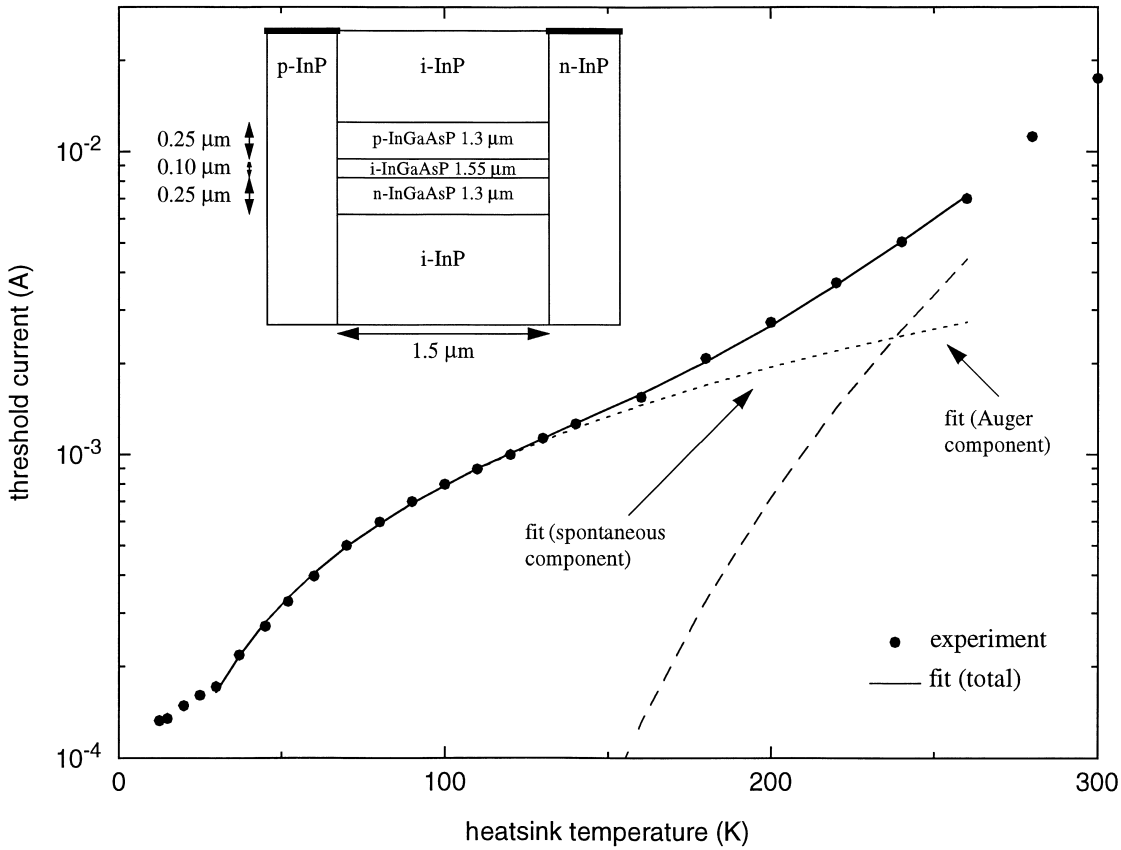

Fig. 21. (Experiment and theory.) Measured threshold current as a function of heatsink temperature, along with curve fit based on a simple physical model incorporating spontaneous and Auger recombination as well as gain — carrier density temperature dependence.

GaInAsP wells were clad by 200 Å 1.25Q p-doped (8×10^{17} cm^{-3}) barriers. This multi-quantum well active region (with room-temperature PL peak at 1585 nm) was clad above and below by *current guides*, 500 Å thick layers of the same composition and doping as the barriers. This structure was in turn sandwiched between 0.5 μm undoped InP cladding layers. A number of remedies to the challenge of ambipolar transport of carriers were incorporated into this epitaxial structure:

- compressively strained quantum wells were used to reduce the heavy-hole effective mass and increase thereby the mobility of the limiting carrier;
- current guiding layers and doped barriers were introduced for 'hybrid' injection of carriers — predominantly lateral injection aided by some vertical carrier flow — into the active region. P-type guides were used to enhance injection of holes, the limiting carrier;
- compressively strained quantum wells were also used in aid of reducing parasitic recombination effects (e.g. Auger recombination);
- many quantum wells were used for a high confinement factor low threshold carrier density. Parasitic effects (e.g. Auger recombination and carrier leakage) were thereby minimized.

The dependence of threshold current, spontaneous efficiency, and stimulated efficiency are given in Fig. 20 for devices with 1 and 2 μm wide ridges. At heatsink temperatures of 50 K and below, the 2 μm device lased in a first-order lateral mode rather than the fundamental mode (observed by measuring the lateral far-field profile). The transition from fundamental- to first-order mode lasing is also manifest in a commensurate jump in threshold current. As discussed above, first-order mode lasing may be favoured over fundamental mode lasing in an LCI laser if the lateral gain profile is strongly nonuniform. The 1 μm wide device exhibits consistent fundamental mode operation from 10 to 300 K, with a continuous decrease in stimulated efficiency below 70 K. The overlap between the single-humped, laterally centered fundamental mode and the nonuni-

form, asymmetric lateral gain profile decreases as the ambipolar diffusion length drops at low temperatures. Further confirmation of lateral gain nonuniformity is obtained by comparing the evolution of threshold current in 1 and 2 μm wide devices (Fig. 20(a)). The 2 μm device exhibits a discontinuous jump in the dependence of threshold current on heatsink temperature commensurate with switching between fundamental and first-order mode lasing; the 1 μm device exhibits a smooth temperature dependence. Close to room-temperature, the threshold current of the 2 μm device exhibits a significant upswing between 270 and 290 K, while the rate of increase of the threshold current of the 1 mm device stays approximately constant on the logarithmic scale up to room-temperature. The more pronounced carrier density nonuniformity in the wider device results in a more rapid increase in superlinear nonradiative current associated with Auger recombination and in a reduced mode-gain overlap. A lower spontaneous efficiency (Fig. 20(b)) in the 1 μm device indicates greater nonradiative recombination due to defects introduced during zinc diffusion. That the spontaneous efficiencies approach one another at higher temperatures implies that Auger recombination begins to dominate over nonradiative mechanism which preponderated at lower temperatures, since Auger recombination is a more strongly temperature-activated process.

5.3. Doubly etched-and-regrown LCI lasers with current guides [70]

The laser of Oe et al. [59] depicted in Fig. 9 was subjected to further experimental and theoretical study. The device lased at 1.55 μm continuous wave at room-temperature with a threshold of 10 mA and optical powers per facet in excess of 10 mW. The key novel feature of this laser — current guides, doped layers of intermediate composition placed above and below the active region — had been shown using two-dimensional fully self-consistent numerical simulation to smooth out the lateral material gain profile in the device, permitting efficient pumping of the fundamental optical mode. Another effect of current guides is to reduce the series resistance of the active region by increasing the area available for the injection of a given current. Resistive heating is decreased as a result, making continuous wave room-temperature operation feasible. In addition, as voltage accumulates more slowly across leakage paths in parallel with the active region, the onset of significant leakage current occurs at higher optical powers.

The epitaxial structure consisted of a 0.1 μm thick undoped bulk active region ($\lambda = 1.55\,\mu m$) clad above and below by 0.25 μm thick n- and p-doped current guides ($\lambda = 1.3\,\mu m$) and undoped InP. p-Type and n-type lateral contacts were formed by dry etching followed by liquid phase epitaxial overgrowth. The device reported in these studies had a 1.5 μm wide active region.

We characterized this device over temperatures ranging from 10 to 300 K. We plot in Fig. 21 the evolution of threshold current with temperature. We derived a simple analytical expression from which to predict the temperature-dependence of the threshold current, assuming (1) that leakage effects were negligible at threshold; (2) that the bulk active region threshold carrier density obeyed an approximate $T^{3/2}$ temperature dependence; (3) that the bimolecular coefficient B obeyed a $T^{-3/2}$ dependence; and (4) that the Auger coefficient C obeyed an exponential characteristic with activation energy 53 meV. As shown in Fig. 21, we obtained excellent agreement between this simple model and experimentally measured threshold currents over the temperature range 30–260 K. Based on the resulting fitting parameters, we estimated the room-temperature bimolecular coefficient and Auger coefficient to be $B = 2 \times 10^{-10}\,cm^3 s^{-1}$ and $C = 5 \times 10^{-28}\,cm^6 s^{-1}$.

The experimental results and fit agree well in the temperature range 40–260 K. At very low temperatures, the temperature dependence of the threshold current levels out rather than continuing the more rapid decrease predicted from simple spontaneous emission/gain considerations. Studying the dependence of threshold voltage on temperature suggested a rapid decrease in ambipolar diffusion length below this critical temperature, resulting in a reduced overlap of gain and fundamental optical mode.

The preceding results point to a number of conclusions relevant to the design of improved lateral current injection lasers. We have found that a nonuniformity in the lateral carrier density may not, on its own, be a source of severe degradation in LCI laser output. It is a related phenomenon — the high series resistance of LCI laser active region — which had a more important impact on device performance in all of the cases considered herein. We have not demonstrated the importance of reducing the *total* series resistance from contact to contact — undoubtedly important if Joule heating is taken into account — but only the resistance across the active region itself.

A number of ways which could be employed in concert in order to postpone the onset of LCI laser efficiency roll-off were identified throughout the course of this combined theoretical–experimental study:

- Increase the aspect ratio of active region thickness to contact separation.
- Maximize p-contact doping in order to minimize the differential resistance of the p-contact-to-active-

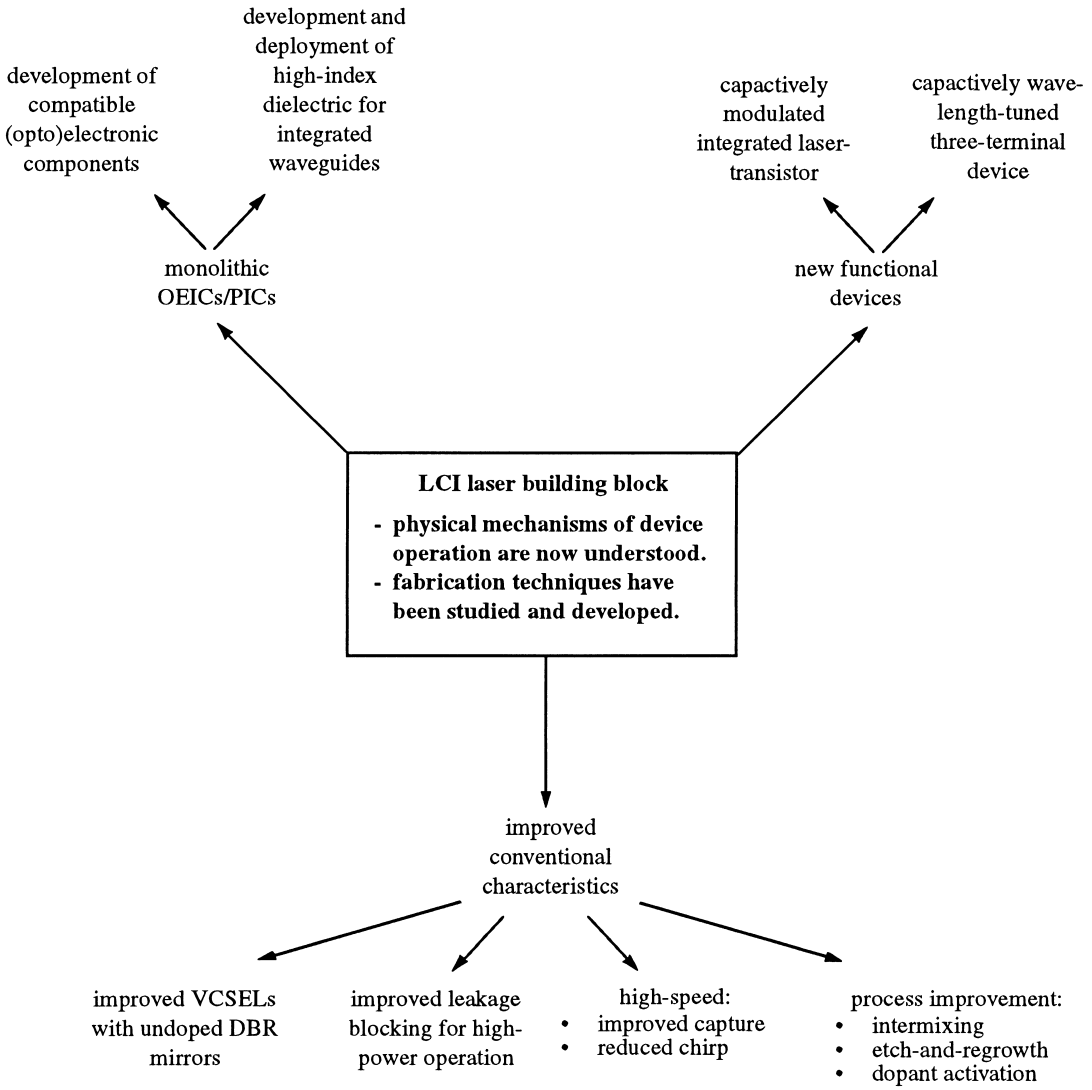

Fig. 22. Future directions and spin-offs from the progress in LCI laser theory and technology.

region heterojunction.

- Maximize the effective area of the injection path for a given current. Current guides — be they doped or undoped (and of a bandgap fairly close to that of the active region) — represent an effective means of reducing the average injected current density for a given injected current. There is of course a trade-off to be found, since using very thick current guides could offset many of the benefits of lateral injection (e.g. reduced free carrier absorption and associated wavelength chirp).
- Increase the ambipolar mobility of the active region. The use of strain-compensated multi-quantum well structures could, by breaking the light-hole/heavy-hole valence band degeneracy, allow lasing primarily on higher mobility light-hole states.
- Increase the resistance of the parasitic paths using a technique such as iron doping of the cladding material.
- Decrease the thickness of *contacted* leakage paths by performing the minimum amount of regrowth required to contact the active region (including current guides) only.

6. Conclusions and future directions

At the outset of this work, the paradigm of vertical injection in semiconductor lasers was set aside and the

assumptions and inertia underlying the present state of semiconductor laser evolution were questioned. While previous researchers have acknowledged the benefits of growth on semi-insulating material, the promise of lateral explorations was shown in this work to reside in a more general property — the release of a new degree of freedom. Vertical injection of carriers necessitates a number of severely limiting compromises — for example, doping must be heavy and uniform throughout the structure. By releasing a new spatial degree of freedom, lateral injection of carriers relaxes many of the mutually constraining requirements inherent to vertical injection.

A predominantly empirical approach to LCI laser development had been adopted in the past. Devices were designed and fabricated using existing principles and technologies. A fresh approach was taken in this work, one free from past assumptions and constraints. Equations describing the interaction of electrons, holes, and photons in a semiconductor medium served as the conceptual foundation for this exploration. An analytical model was developed and applied. Fully self-consistent modelling of specific representative devices permitted a more complete accounting of the interactions of carriers and photons in two dimensions. Process development for quantum well intermixing, dry etching, epitaxial regrowth, doping by ion implantation, and ohmic contact development were required prior to laser fabrication. LCI lasers were fabricated using two promising fabrication streams. A range of devices was characterized electrically and optically over a broad range of temperatures. By exploring device behaviour with respect to this added adjustable parameter, the internal operating mechanisms predicted, explained and modelled were validated experimentally.

The understanding and technologies developed pave the way for further exploration of the fundamental mechanisms underlying LCI laser operation; of practical and reliable technologies for enabling successful device fabrication; and of the potential for creating novel functional devices and monolithic OEICs. Areas for further exploration are depicted in Fig. 22 and are discussed briefly.

6.1. Further progress in lateral injection laser theory

A matter of great theoretical and practical interest is the nature of carrier injection from three-dimensional states in bulk contacts to lower-dimensional states in quantum-confined structures such as wells and wires. In vertical injection structures, this is one mechanisms responsible for limiting the speed of direct laser modulation: carriers must lose substantial momentum in their direction of propagation. In the lateral geometry, however, carriers may preserve their momentum in the direction of travel. In either lateral or vertical injection, injected carriers must relax into energetic states wherein they may contribute to optical gain at the lasing wavelength. In vertical injection devices, carriers typically experience large, sudden changes in band energies as they move along their vertical trajectory. The lateral injection paradigm offers the possibility of preserving an abrupt heterostructure in the vertical direction in order to maximize quantum confinement, while simultaneously permitting a more gradual energetic transition along the lateral path of carriers. Such an adiabatic lateral transition from 3D injector states into 2D active region states arises naturally by virtue of a lateral grading of the band structure in LCI lasers fabricated using quantum well intermixing.

The dynamic operation of the LCI laser is a further area of great interest. The LCI laser merits study on this front for reasons of general interest, since qualitative mechanisms may differ significantly from those which limit vertical injection lasers. It is also particularly promising from a technological standpoint: high-speed direct modulation of semiconductor lasers (40 GHz and beyond) is desired in telecommunications applications, but suffers in the vertical injection paradigm from excessive wavelength chirp. Although vertical injection lasers have been made which meet bandwidth requirements [5], simultaneous modulation of the density of free carriers in the cladding and separate confinement heterostructure regions gives rise to a commensurate modulation in the wavelength of emitted light. Free carriers need only be injected (and therefore modulated) where they are needed in the LCI laser — the quantum wells.

There may also be substantial advantages in lateral injection with respect to the ease with which high modulation bandwidths may be achieved. The lateral injection approach permits a substantial reduction in capacitance due to the collinear contact geometry and undoped substrate. The planar nature of LCI laser technology is directly compatible with microwave stripline interconnections. A third, less straightforward consideration relates to carrier transport. In vertical lasers, the effective travel time is increased by multiple quantum well carrier capture and escape processes. The LCI approach has the advantage of reducing the capture–escape problem, as carriers travel along the quantum wells rather than across them. Moreover, the two-dimensional bipolar lateral transport along the quantum wells might be faster due to the reduced dimensionality of the system. There are thus indications that the speed limit of LCI lasers can actually exceed that of the vertical injection lasers, despite a seemingly longer carrier travel path in the active region of the LCI structures.

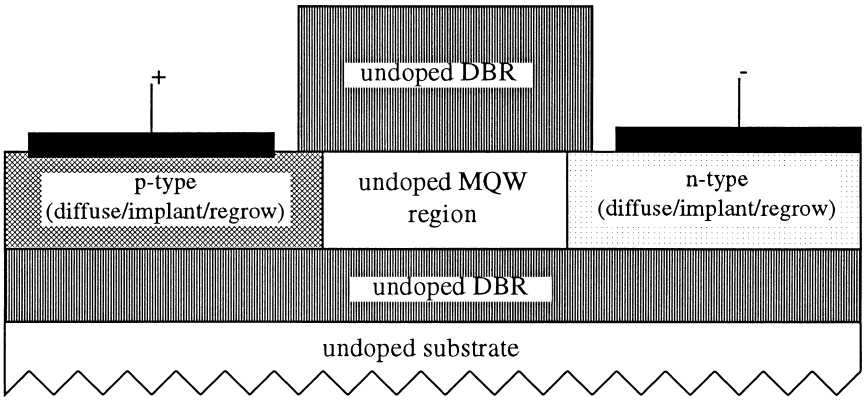

Fig. 23. Proposed lateral injection VCSEL.

6.2. Further progress in planar laser fabrication

Lateral heterobarrier formation by ion mixing needs to be further developed so that substantial heterobarriers may be created reproducibly in order to improve carrier confinement. Contacts must be doped to a high level and residual damage must be largely removed. The series resistance associated with metal–semiconductor contacts and bulk semiconducting regions is also an important experimental feature needing further study and control.

A possible etch-free regrown-LCI laser process also deserves exploration. Damage created in a semiconductor during dry etching is a serious concern for etch-and-regrowth processing. As an alternative, selective-area growth (SAG) permits planar differentiation without recourse to damaging dry etching. Such a process would begin with selective growth of the laser active region on a dielectric-masked wafer surface. The mask would be removed, and a buried heterostructure formed by an additional growth atop this structure. One useful feature of this approach is that the properties of the dielectric mask pattern influence the rate of growth of the active region; lasers with controlled differences in wavelength may therefore be grown simultaneously.

6.3. Novel device explorations

LCI lasers permit the use of an insulating vertical heterostructure and therefore lend themselves to control via the application of an electric field using a third terminal. This electrical field could be used to modulate the injection of current by controlling the conductivity of the channel. Alternatively, an electric field could be applied across the active region to tune the energy levels in the quantum wells, thereby permitting tuning of the gain spectrum and the laser emission spectrum. The further possibility of placing an additional quantum well under the gate would allow capacitive modulation of the absorption or confinement factor.

Certain challenges remain to be addressed before these attractive possibilities become a reality. A study of the fundamental limits of modulation speed is needed to establish that the advantages of these devices extend beyond intrinsic integrability into the realm of improved dynamic performance.

The release of the lateral direction also holds great promise for improved vertical cavity surface-emitting laser (VCSELs). Progress in VCSEL development, particularly at longer wavelengths, is presently hampered by the fact that carrier injection and optical feedback are both achieved in the vertical direction. In VCSELs, a pair of distributed Bragg reflectors (DBR) is typically used to create high reflectivity mirrors. The heterostructure associated with these DBRs increases the resistance of the medium through which current must be injected in order to reach the active region. Doping in the DBRs must be kept to a moderate level if free-carrier absorption is not to be unduly severe. The need for this compromise highlights the constraining nature of the purely vertical approach.

IIn VCSELs intended for long-wavelength operation, vertical injection suffers another drawback. A recent breakthrough in long-wavelength VCSEL technology has been the introduction of wafer fusion: mirrors are grown in the high-index-contrast AlGaAs/GaAs system and are fused to a GaInAsP-based active region wafer [99]. This wafer-fused interface is acceptable from an optical standpoint, but results in tremendous increases in threshold voltage. The lateral injection VCSEL portrayed in Fig. 23 would address many of these issues in a natural and convenient manner. In particular, it would allow:

- the use of completely intrinsic DBR mirrors for very low free-carrier absorption;
- the use of heavily-doped injectors;

- current to be injected along a path which would circumvent the fused interface entirely;
- multi-quantum well structures to be placed at several standing wave peaks of the vertically-confined optical mode. Because of restrictions on active region thickness in conventional VCSELs, gain regions are typically placed at only one standing wave peak. As a result, the threshold carrier density is high and L–I characteristics usually degrade at low optical powers.

If the planar dimension can be better employed in lateral injection lasers, opportunities in the longitudinal direction merit exploration as well. A more uniform distribution of carriers and photons could be achieved by varying the coupling strength of a DFB grating along its length. In vertical injection structures, it is difficult to modify the grating strength without simultaneously modifying the resistance. As argued previously, lateral injection of current enables a decoupling of these two factors so that feedback strength and injection strength could be controlled independently. Further exploration along the longitudinal dimension is also promising for the development of split electrode devices which would not suffer from undesired electrical coupling as they do in the vertical injection paradigm.

References

[1] Steele R. Review and forecast of laser markets: 1998. II. Laser Focus World, 1998, February, 72–93.

[2] McDaniel MR, Huffaker DL, Deppe DG. Hybrid dielectric/metal reflector for low threshold vertical-cavity surface-emitting lasers. Electron Lett 1997;33:1704–5.

[3] Groves SH, Walpole JN, Missaggia LJ. Very high efficiency GaInAsP/GaAs strained-layer quantum well lasers ($\lambda = 980$ nm) with GaInAsP optical confinement layers. Appl Phys Lett 1992;61:255–7.

[4] Smith GM, Hughes JS, Lammert RM, Osowski ML, Papen GC, Verdeyen JT, Coleman JJ. Wavelength-tunable asymmetric cladding ridge-waveguide distributed Bragg reflector lasers with very narrow linewidth. IEEE J Quantum Electron 1996;32:1225–9.

[5] Zhang X, Gutierrez-Aitken A, Klotzkin D, Bhattacharya P, Caneau C, Bhat R. 0.98 μm multiple-quantum-well tunneling injection laser with 98 GHz intrinsic modulation bandwidth. IEEE J Selected Topics Quantum Electron 1997;3:309–14.

[6] Braun E, Macdonald S. Revolution in miniature: the history and impact of semiconductor electronics. New York: Cambridge University Press, 1982.

[7] Morton JA. From physics to function. In: IEEE Spectrum, 1965. p. 62–6.

[8] Namizaki H, Kan H, Ishii M, Ito A. Transverse-junction-stripe-geometry double-heterostructure lasers with very low threshold current. J Appl Phys 1974;45:2785–6.

[9] Namizaki H. Transverse-junction-stripe-geometry double-heterostructure lasers with a GaAs p–n homojunction. IEEE J Quantum Electron 1975;QE-11:427–31.

[10] Namizaki H, Ishii M, Kan H, Ohmura E, Hirano R, Ito A. Long-life GaAs–GaAlAs TJS laser with low threshold current and fundamental transverse and single longitudinal mode. Optics Communications 1976;18:39–40.

[11] Susaki W, Tanaka T, Kan H, Ishii M. New structures of GaAlAs lateral-injection laser for low-threshold and single-mode operation. IEEE J Quantum Electron 1977;QE-13:587–91.

[12] Oomura E, Hirano R, Tanaka T, Ishii M, Susaki W. Laser with buried p-region for high temperature cw operation. IEEE J Quantum Electron 1978;QE-14:460–1.

[13] Kumabe H, Tanaka T, Namizaki H, Ishii M, Susaki W. High temperature single-mode cw operation with a junction-up TJS laser. Appl Phys Lett 1978;33:38–9.

[14] Isshiki K, Kaneno N, Kumabe H, Namizaki H, Ikeda K, Susaki W. Ten-thousand-hour operation of crank transverse-junction-stripe lasers grown by metal-organic chemical vapor deposition. IEEE J Lightwave Technol 1986;LT-4:1475–81.

[15] Mitsunaga K, Fujiwara K, Nunoshita M, Nakayama T. Si-doped GaAs/AlGaAs TJS laser by MBE. J Vac Sci Technol B 1984;2:256–8.

[16] Nita S, Namizaki H, Takamiya S, Susaki W. Single-mode junction-up TJS lasers with estimated lifetime of 10^6 h. IEEE J Quantum Electron 1979;QE-15:1208–9.

[17] Kadota Y, Chino K, Onodera Y, Namizaki H, Takamiya S. Aging behavior and surge endurance of 870–900 nm AlGaAs lasers with nonabsorbing mirrors. IEEE J Quantum Electron 1984;QE-20:1247–51.

[18] Kumabe H, Nita S, Seiwa Y, Tanaka T, Sogo T, Horiuchi S, Takamiya S. Continuous-wave 15 mW operation test of single-mode high-power crank structure TJS laser diodes. In: Conference on Lasers and Electro-Optics (CLEO '81). 1981. p. 152–3.

[19] Namizaki H, Kumabe H, Susaki W. Spontaneous emission behavior in AlGaAs TJS lasers. IEEE J Quantum Electron 1981;QE-17:799–803.

[20] Nagai S, Nita S, Yamashita K, Sogo T, Takamiya S. Noise characteristics of multi-longitudinal-mode transverse junction stripe laser diodes. In: 9th European Conference on Optical Communication. 1983. p. 143–6.

[21] Kumabe H, Isshiki K, Namizaki H, Nishioka T, Koyama H, Takamiya S. Mechanical stress suppressed AlGaAs high power TJS laser diodes. In: 15th Conference on Solid State Devices and Materials. 1983. p. 329–32.

[22] Yang YJ, Lo YC, Lee GS, Hsieh KY, Kolbas RM. Transverse junction stripe laser with a lateral heterobarrier by diffusion enhanced alloy disordering. Appl Phys Lett 1986;49:835–7.

[23] Sin Y, Hsieh KY, Lee JH, Kolbas RM. Surface and bulk leakage currents in transverse junction stripe lasers. J Appl Phys 1991;69:1081–90.

[24] Yu KL, Koren U, Chen TR, Yariv A. Groove GaInAsP laser on semi-insulating InP using a laterally diffused junction. IEEE J Quantum Electron 1982;QE-18:817–9.

[25] Chen TR, Koren U, Yu KL, Lau KY, Chiu LC, Hasson A, Margalit S, Yariv A. High-power, single-mode operation of an InGaAsP/InP laser with a grooved transverse

junction using gain stabilization. Appl Phys Lett 1982;41:225–8.
[26] Chang LB, Shia LZ. Room-temperature continuous wave operation of a visible AlGaAs/InGaP transverse junction stripe laser grown by liquid phase epitaxy. Appl Phys Lett 1992;60:1090–2.
[27] Chang LB, Shai LZ. Fabrication methods for an AlGaAs/InGaP/AlGaAs visible laser with transverse junction stripe structure grown by liquid phase epitaxy. Solid State Electron 1993;36:1049–54.
[28] Ishii M, Kamon K, Shimazu M, Mihara M, Kumabe H, Isshiki K. Planar TJS lasers fabricated in semi-insulating GaAs substrates for optoelectronic integrated circuits. Electron Lett 1987;23:179–81.
[29] Ohta J, Kuroda K, Mitsunaga K, Kyuma K, Hamanaka K, Nakayama T. Buried transverse-junction stripe laser for optoelectronic-integrated circuits. J Appl Phys 1987;61:4933–5.
[30] Ohta J, Kuroda K, Mitsunaga K, Kyuma K, Hamanaka K, Nakayama T. Monolithic integration of a transverse-junction stripe laser and metal-semiconductor field-effect transistors on a semi-insulating GaAs substrate. Electron Lett 1987;23:509–10.
[31] Brillouet F, Rao EVK, Beerens J, Gao Y. A new low capacitance transverse junction stripe AlGaAs/GaAs laser for planar laser-MESFET integration. In: Proceedings of the 14th International Symposium on Gallium Arsenide and Related Compounds, 1987. p. 789–92.
[32] Brillouet F, Rao EVK, Beerens J. New low capacitance transverse junction stripe AlGaAs/GaAs laser for planar laser-MESFET integration. Electron Lett 1988;24:97–9.
[33] Honda Y, Suemune I, Yamanishi M. Monolithic integration of a lateral current injection laser and a JFET based on the same modulation doped structure. In: 22nd Conference on Solid State Devices and Materials. 1990. p. 1179–80.
[34] Yasuhira N, Suemune I, Kan Y, Yamanishi M. Selectively doped double-heterojunction lateral current injection ridge waveguide AlGaAs/GaAs laser. Appl Phys Lett 1990;56:1391–3.
[35] Honda Y, Suemune I, Yasuhira N, Yamanishi M. new optoelectronic device based on modulation-doped heterostructure: demonstration of functions as both lateral current injection laser and junction field effect transistor. IEEE Photon Technol Lett 1990;2:881–3.
[36] Honda Y, Suemune I, Yasuhira N, Yamanishi M. Continuous-wave operation of lateral current injection ridge waveguide AlGaAs/GaAs laser with a selectively-doped heterostructure. 1. Jpn J Appl Phys 1991;30:990–1.
[37] Evaldsson PA, Taylor GW, Cooke P, Claisse PR, Burrus CA, Tell B. Small-signal and continuous wave operation of the lateral current injection heterostructure field-effect laser. Appl Phys Lett 1992;60:1697–9.
[38] Sargood SK, Taylor GW, Claisse PR, Vang T, Cooke P, Docter DP, Kiely PA, Burrus Jr. CA. quantum-well inversion channel heterostructure as a multifunctional component for optoelectronic integrated circuits. IEEE J Quantum Electron 1993;29:136–49.
[39] Vawter GA, Merz JL, Coldren LA. Monolithically integrated transverse-junction-stripe laser with an external waveguide in GaAs/AlGaAs. IEEE J Quantum Electron 1989;25:154–62.
[40] Kawanishi H, Hafich M, Lenz B, Petersen P. AlGaAs transverse junction stripe laser with distributed Bragg reflector. Electron Lett 1980;16:738–40.
[41] Kawanishi H, Hafich MJ, Skogman RA, Lenz BS, Petersen PE. GaAs/AlGaAs distributed feedback-transverse junction stripe laser using a hybrid liquid phase epitaxy/metal-organic chemical vapor deposition growth technique. J Appl Phys 1981;52:4447–9.
[42] Kyuma K, Tai S, Nunoshita M. Fiber-optic laser Doppler velocimeter using an external-cavity semiconductor laser. In: Conference on Optical Fiber Communication. 1984. p. 58–9.
[43] Kameya M, Tai S, Mitsunaga K, Kyuma K, Hamanaka K, Nakayama T. Spectral linewidth of an AlGaAs/GaAs DFB-TJS external-cavity laser with optical phase control loop. Electron Lett 1986;22:1231–2.
[44] Mitsunaga K, Noda S, Kojima-K K, Kameya M, Kyuma K, Hamanaka K, Nakayama T. GaAs/AlGaAs distributed feedback transverse junction stripe laser grown by molecular beam epitaxy. Appl Phys Lett 1987;50:1622–4.
[45] Hsin W, Ogura M, Weber JP, Wang SC, Yang JJ, Wu MC, Wang S, Whinnery JR. GaAs/AlGaAs surface emitting laser diode with vertical distributed feedback optical cavity and transverse junction buried heterostructure. IEDM Technical Digest, 1987. p. 792–5.
[46] Yamada H, Watanabe H, Ito H, Inaba H. Surface-emitting GaAs light-emitting diode/laser diode with modified coaxial transverse junction (CTJ) structure. Electron Lett 1988;24:77–8.
[47] Mitsunaga L, Kameya M, Kojima K, Noda S, Kyuma K, Hamanaka K, Nakayama T. surface-emitting grating-coupled GaAs/AlGaAs distributed feedback laser with very narrow beam divergence. Appl Phys Lett 1987;50:1788–90.
[48] Takamori T, Coldren LA, Merz JL. Folded-cavity transverse junction stripe surface-emitting laser. Appl Phys Lett 1989;55:1053–5.
[49] Yang W, Gopinath A, Hibbs-Brenner M. Planar GaAs–AlGaAs MQW transverse junction ridge waveguide lasers using shallow zinc diffusion. IEEE Photon Technol Lett 1995;7:848–50.
[50] Furuya A, Makiuchi M, Wada O, Fujii T, Nobuhara H. AlGaAs/GaAs lateral current injection (LCI)-MQW laser using impurity-induced disordering. Jpn J Appl Phys 1987;26:L134–135.
[51] Furuya A, Makiuchi M, Wada O. Continuous-wave operation of lateral current injection multiquantum-well laser. Electron Lett 1988;24:1282–3.
[52] Furuya A, Makiuchi M, Wada O, Fujii T. AlGaAs/GaAs lateral current injection multiquantum well (LCI-MQW) laser using impurity-induced disordering. IEEE J Quantum Electron 1988;24:2448–53.
[53] Wada O, Furuya A, Makiuchi M. Planar, compatible OEIC's based on multiquantum well structures. IEEE Photon Technol Lett 1989;1:16–8.
[54] Suzuki Y, Mukai S, Yajima H, Sato T. Transverse junction buried heterostructure (TJ-BH) AlGaAs diode laser. Electron Lett 1987;23:384–6.

[55] Shimoyama K, Katoh M, Noguchi M, Inoue Y, Gotoh H, Suzuki Y, Satoh T. Transverse junction buried heterostructure (TH-BH) laser diode grown by MOVPE. J Crystal Growth 1988;93:803–8.
[56] Shimoyama K, Katoh M, Suzuki Y, Satoh T, Inoue Y, Nagao S, Gotoh H. Operation and extremely low capacitance of TJ-BH MQW laser diodes fabricated by entire MOVPE. Jpn J Appl Phys 1988;27:L2417–L2419.
[57] Shimoyama K, Katoh M, Suzuki Y, Satoh T, Inoue Y, Nagao S, Gotoh H. CW operation and extremely low capacitance of TJ-BH laser diodes having MQW active layers fabricated by entire MOVPE. In: 20th Conference on Solid State Devices and Materials. 1988. p. 343–6.
[58] Kawamura Y, Noguchi Y, Iwamura H. Lateral current injection InGaAs/InAlAs MQW lasers grown by GSMBE/LPE hybrid method. Electron Lett 1993;29:102–3.
[59] Oe K, Noguchi Y, Caneau C. GaInAsP lateral current injection lasers on semi-insulating substrates. IEEE Photon Technol Lett 1994;6:479–81.
[60] Sargent EH, Tan GL, Xu JM. Investigations of lateral current injection lasers: internal operating mechanisms and doping profile engineering. In: Compound Semiconductors 1996, 1996. p. 651–4.
[61] Sargent EH, Tan GL, Suda DA, Xu JM. Internal operating mechanisms of OEIC-compatible lateral injection lasers: intrinsic differences from the vertical injection paradigm. In: 15th IEEE International Semiconductor Laser Conference. 1996. p. 111–2.
[62] Sargent EH, Xu JM. Investigations of the physical mechanisms governing the performance of OEIC-compatible p–i–n active region lateral current injection lasers. In: LEOS '96 Annual Meeting, 1996. p. 314–5.
[63] Sargent EH, Tan GL, Xu JM. Physical model of OEIC-compatible lateral current injection lasers. IEEE Journal of Selected Topics in Quantum Electronics 1997;3:507–12.
[64] Sargent EH, Xu JM. Integration-compatible lateral current injection lasers: design of 2D heterostructure devices. In: Conf. on Lasers and Electro-Optics/Pacific Rim. 1997.
[65] Sargent EH, Caneau C, Zah C, Xu JM. OEIC-Enabling Lateral Current Injection Lasers: Underlying Physics Mechanisms and Design for Improved High-Power Efficiency. In: International Topical Workshop on Contemporary Photonic Technologies, 1998.
[66] Sargent EH, Tan G, Xu JM. Lateral current injection lasers: underlying mechanisms and design for improved high-power efficiency. Journal of Lightwave Technology 1998;16(10):1854–64.
[67] Sargent EH, Meshkati F. OEIC-enabling lateral current injection (LCI) lasers: efficient functional devices using lateral beam-steering. In: European Conference on Integrated Optics. 1999.
[68] Sargent EH, Xu JM, Caneau C, Zah C. Experimental investigation of physical mechanisms underlying lateral current injection laser operation. Appl Phys Lett 1998;73:285–7.
[69] Sargent EH, Suda DA, Margittai A, Shepherd FR, Cleroux M, Knight G, Puetz N, Makino T, SpringThorpe AJ, Chik G, Xu JM. Experimental study of LCI lasers fabricated by single MOCVD overgrowth followed by selective dopant diffusion. IEEE Photon Technol Lett 1998;10(11):1536–8.
[70] Sargent EH, Oe K, Caneau C, Xu JM. OEIC-enabling LCI lasers with current guides: combined theoretical-experimental investigation of internal operating mechanisms. IEEE J Quantum Electron 1998;34:1280–7.
[71] Matsushita K, Hartnagel HL. Plasma etching of InP. In: Properties of Indium Phosphide. New York: INSPEC, 1991.
[72] Pearton SJ. Ion beam processing and rapid thermal annealing of InP and related compounds. In: Second International Conference on Indium Phosphide and Related Materials. 1990. p. 379–88.
[73] Miyakuni S, Hattori R, Sato K, Takano H, Ishihara O. Low ion energy electron cyclotron resonance etching of InP using Cl_2/N_2 mixture. J Appl Phys 1995;78:5734–8.
[74] Ryssel H, Ruge I. Ion implantation. New York: Wiley, 1986.
[75] Bahir G, Merz JL. Rapid Thermal Annealing and Solid Phase Epitaxy of Ion Implanted InP. SPIE Vol. 623, Advanced Processing and Characterization of Semiconductors. III, 1986. p. 149–56.
[76] Sealy BJ. Ion implantation of InP: overview. In: Properties of indium phosphide. New York: INSPEC, 1991.
[77] Hailemariam E, Pearton SJ, Hobson WS, Luftman HS, Perley AP. Doping of $In_{0.53}Ga_{0.47}As$ and $In_{0.52}Al_{0.48}As$ by Si^+ and Be^+ ion implantation. J Appl Phys 1992;71:215–20.
[78] Elenkrig BB, Thompson DA, Simmons JG, Bruce DM, Si Y, Zhao J, Evans JD, Templeton IM. Experimental study of implantation-induced disordering in InGaAsP strained multiple-quantum-well heterostructures. Appl Phys Lett 1994;65:1239–41.
[79] Rao MV, Nadella RK. Be^+/P^+, Be^+/Ar^+ and Be^+/N^+ coimplantations into InP:Fe. J Appl Phys 1990;67:1761–6.
[80] Christel LA, Gibbons JF. Stoichiometric disturbances in ion implanted compound semiconductors. J Appl Phys 1981;52:5050–5.
[81] Heckingbottom R, Ambridge T. Ion implantation in compound semiconductors — an approach based on solid state theory. Radiat Eff 1973;17:31–6.
[82] Rao EVK, Hamoudi A, Krauz P, Juhel M, Thibierge H. New encapsulant source for III–V quantum well disordering. Appl Phys Lett 1995;66:472–4.
[83] Marsh JH, Bryce AC. Quantum well intermixing for optoelectronic integration. Proceedings-of-the-SPIE 1994;2139:72–80.
[84] Tell B, Shah J, Thomas PM, Brown-Goebeler KF, DiGiovanni A, Miller BI, Koren U. Phosphorus ion implantation induced intermixing of InGaAs–InP quantum well structures. Appl Phys Lett 1989;54:1570–2.
[85] Poole PJ, Charbonneau S, Aers GC, Jackman TE, Buchanan M, Dion M, Goldberg RD, Mitchell IV. Defect diffusion in ion implanted AlGaAs and InP: Consequences for quantum well intermixing. J Appl Phys 1995;78:2367–71.
[86] Elenkrig BB, Thompson DA, Simmons JG, Bruce DM, Si Y, Zhao J, Evans JD, Templeton IM. Experimental

study of implantation-induced disordering in InGaAsP strained multiple-quantum-well heterostructures. Appl Phys Lett 1994;65:1239–41.

[87] Wan JZ, Simmons JG, Thompson DA. Band gap modification in Ne^{+}-ion implanted $In_{1-x}Ga_xAs/InP$ and $InAs_yP_{1-y}/InP$ quantum well structures. J Appl Phys 1997;81:765–70.

[88] Dreybrodt J, Oshinowo J, Forchel A, Emmerling M, Gyuro I, Speier P, Zielinski E. High resolution definition of buried $In_{0.53}Ga_{0.47}As/InP$ wires by implantation induced intermixing. In: 4th International Conference on Indium Phosphide and Related Materials. 1992. p. 63–6.

[89] Mito I, Kitamura M, Kaede K, Odagiri Y, Seki M, Sugimoto M, Kobayashi K. InGaAsP planar buried-heterostructure laser diode (PBH-LD) with very low threshold current. Electron Lett 1982;18:2–3.

[90] Bhat R. Current status of selective area epitaxy by OMCVD. J Crystal Growth 1992;120:362–8.

[91] Zwinge G, Wehmann H-H, Schlachetzki A, Hsu CC. Orientation-dependent growth of InGaAs/InP for applications in laser-diode arrays. J Appl Phys 1993;74:5516–8.

[92] Frei MR, Hayes JR, Shirokmann HF, Caneau C. Regrowth of $In_{0.53}Ga_{0.47}As/InP$ p–n heterojunctions by organometallic chemical vapor deposition. J Appl Phys 1991;70:3967–9.

[93] Yablonovitch E, Bhat R, Zah CE, Gmitter TJ, Koza MA. Nearly ideal $InP/In_{0.53}Ga_{0.47}As$ heterojunction regrowth on chemically prepared $In_{0.53}Ga_{0.47}As$ surfaces. Appl Phys Lett 1992;60:371–3.

[94] Heime K. InGaAs field-effect transistors. New York: Wiley, 1989.

[95] Wang LC, Park M-H, Deng F, Clawson A, Lau SS, Hwang DM, Palmstrom CJ. Ge/Pd (An) ohmic contact scheme on p-InP based on the solid phase regrowth principle. Appl Phys Lett 1995;66:3310–2.

[96] Morais, Fazan TA, Landers R, Sato EAS. Ohmic contacts formation on n-InP. J Appl Phys 1996;79:7058–61.

[97] Katz A, Thomas PM, Chu SNG, Dautremont-Smith WC, Sobers RG, Napholtz SG. Pt/Ti ohmic contact to p-InGaAsP (1.3 μm) formed by rapid thermal processing. J Appl Phys 1990;67:884–9.

[98] Huelsman AD, Fonstad CG. Fabrication and characterization of nonalloyed Cr/Au ohmic contacts to n- and p-type $In_{0.53}Ga_{0.47}As$. IEEE Trans Electron Devices 1986;ED-33:294–7.

[99] Margalit NM, Babic DI, Streubel K, Mirin RP, Naone RL, Bowers JE, Hu EL. Submilliamp long wavelength vertical cavity lasers. Electron Lett 1996;32:1675–7.